Geophys. J. Int. (2009) doi: 10.1111/j.1365-246X.2009.04229.x

Seismic structure of the southern Apennines as revealed by waveform modelling of regional surface waves

Ahmet Ökeler,[1] Yu Jeffrey Gu,[1] Arthur Lerner-Lam[2] and Michael S. Steckler[2]

[1]*Department of Physics, University of Alberta, Edmonton, AB,* T6G2G7, *Canada. E-mail: aokeler@phys.ualberta.ca*
[2]*Lamont-Doherty Earth Observatory,* 61 *Route 9W, P.O. Box* 1000, *Palisades,* NY 10964, *USA*

Accepted 2009 April 24. Received 2009 April 22; in original form 2009 January 19

SUMMARY

We investigate the crust and upper-mantle structures beneath the southern Apennine mountain chain using three-component seismograms from the Calabria-Apennine-Tyrrhenian/Subduction-Collision-Accretion Network (CAT/SCAN) array. Surface wave waveforms from three moderate-sized ($M_w > 5.0$) regional earthquakes are modelled using multiple frequencies (0.03–0.06 and 0.05–0.2 Hz) and both forward and linearized-inversion algorithms. Our best-fitting shear velocity models clearly reflect the major tectonic units where, for example, the average seismic structure at depths above 50 km beneath Apulia is substantially faster than beneath the Apennine mountain chain. We identify a prominent low-velocity channel under the mountain belt at depths below ∼25–30 km and a secondary low-velocity zone at 6–12 km depth near Mt Vulture (a once active volcano). Speed variations between Love and Rayleigh waves provide further constraints on the fabric and dynamic processes. Our analysis indicates that the crustal low-velocity zones are highly anisotropic (maximum 14 per cent) and allow transversely polarized shear waves to travel faster than vertically polarized shear waves. The upper crustal anomaly reveals a layer of highly deformed rocks caused by past collisions and by the active normal faults cutting across the thrust sheets, whereas hot mantle upwelling may be responsible for a high-temperature, partially molten lower crust beneath the southern Apennines.

Key words: Surface waves and free oscillations; Seismic anisotropy; Wave propagation; Dynamics of lithosphere and mantle; Crustal structure; Europe.

1 INTRODUCTION

The present-day picture of the western Mediterranean region highlights the last stage of continent–continent orogeny (Cavazza *et al.* 2004). The closure of the Mesozoic Neo-Tethyan basins in the Mediterranean region due to north–south (N–S) convergence between Africa and Europe produced a series of subduction and collisional tectonic regimes along the Mediterranean region consisting of the western Mediterranean Subduction Zone, Hellenic Arc, Gibraltar Arc, Alps, Apennines and Zagros Suture Zone (Stampfli & Borel 2004). The western Mediterranean Subduction Zone collided with Sicily in the south and Adria in the northeast, forming the Maghrebides nappes and the Apennine mountain chain, respectively. The southern Apennines, the target area of this study, postdated their northern counterpart in the latest episodes of shortening when active subduction was reduced to the 200-km-wide Calabrian Arc (Hippolyte *et al.* 1994; Carminati *et al.* 1998; Rosenbaum & Lister 2004). After the mid-Pleistocene (Rosenbaum & Lister 2004), evidence from GPS measurements (Hollenstein *et al.* 2003; Serpelloni *et al.* 2005; Serpelloni *et al.* 2006), earthquake depths (Meletti *et al.* 2000; Chiarabba *et al.* 2005), focal mechanisms (Pondrelli *et al.* 2002; Pondrelli *et al.* 2006) and stress orientations (Hippolyte *et al.* 1994; Montone *et al.* 2004) consistently suggest the cessation of subduction/rollback of the Adriatic microplate and the development of extensional forces in the southern Apennines.

So far, the tectonic imprints beneath the southern Apennines have largely been inferred from continental-scale seismic tomography using body and surface wave records (Snieder 1988; Spakman *et al.* 1993; de Jonge *et al.* 1994; Marquering & Snieder 1996; Bijwaard *et al.* 1998; Wortel & Spakman 2000; Marone *et al.* 2003; Piromallo & Morelli 2003; Boschi *et al.* 2004; Spakman & Wortel 2004; Boschi *et al.* 2008). The lateral (100–500 km) and depth (50–100 km) resolutions of these studies are generally too coarse to reveal the detailed seismic signature of the southern Apennines. Such resolution issues are partially overcome by regional-scale *P*/*S* wave tomography (Amato *et al.* 1993; Selvaggi & Chiarabba 1995; Chiarabba & Amato 1996; Di Stefano *et al.* 1999; Lucente *et al.* 1999; Cimini & De Gori 2001; Barberi *et al.* 2004; Montuori *et al.* 2007) and Pn/Sn analyses (Mele *et al.* 1996, 1997, 1998), but

the modest vertical resolution of body waves remains problematic. Recent one-dimensional (1-D) surface wave group and phase velocity inversions (Pentevivo & Panza 2002; Panza *et al.* 2003; Pentevivo & Panza 2006; Panza *et al.* 2007) offer greater depth constraints on the crust/upper-mantle depths; despite the lack of station coverage from permanent networks the horizontal 'block' widths in these surface wave studies are on the order of 100–200 km.

This study presents new seismic constraints on shear velocity and anisotropy at lithospheric depths beneath the southern Apennines. Our analysis is motivated by the Calabria-Apennines-Tyrrhenian/Subduction-Collision-Accretion Network (CAT/SCAN) project, the largest temporary broadband seismic deployment in this region to date. The field project was conducted by a group of researchers from Lamont-Doherty Earth Observatory, the

Table 1. Earthquake parameters reported by Global-CMT, SED and Mednet institutions for three moderate-sized events recorded by CAT/SCAN array.

ID	Date (yr-month-day)	Time (GMT)	Longitude	Latitude	Depth (km)	Magnitude (M_w)	Institution
Event 1	**2005-01-31**	**01:05:35.1**	**19.97**	**37.37**	**12.0**	**5.7**	**Global-CMT**
		01:05:33	**20.155**	**37.535**	**24.0**	**5.78**	**SED**
		01:05:26.1	**20.10**	**37.43**	**19.0**	**5.7**	**Mednet-RCMT**
Event 2	**2004-11-25**	**06:21:22.4**	**15.22**	**43.15**	**12.0**	**5.3**	**Global-CMT**
		06:21:19	**15.364**	**43.167**	**4.0**	**5.3**	**SED**
		06:21:18.7	**15.16**	**43.13**	**15.0 (fixed)**	**5.2**	**Mednet-RCMT**
Event 3	2004-05-05	13:39:47.3	14.75	38.61	238.9	5.5	Global-CMT
		13:39:43	14.814	38.507	255.0	5.47	SED
		13:39:40.6	14.73	38.63	252.0	5.5	Mednet-RCMT

Note: Only events in bold offer sufficient-quality surface waves for waveform modelling. The focal mechanism solutions are shown in Fig. 1.

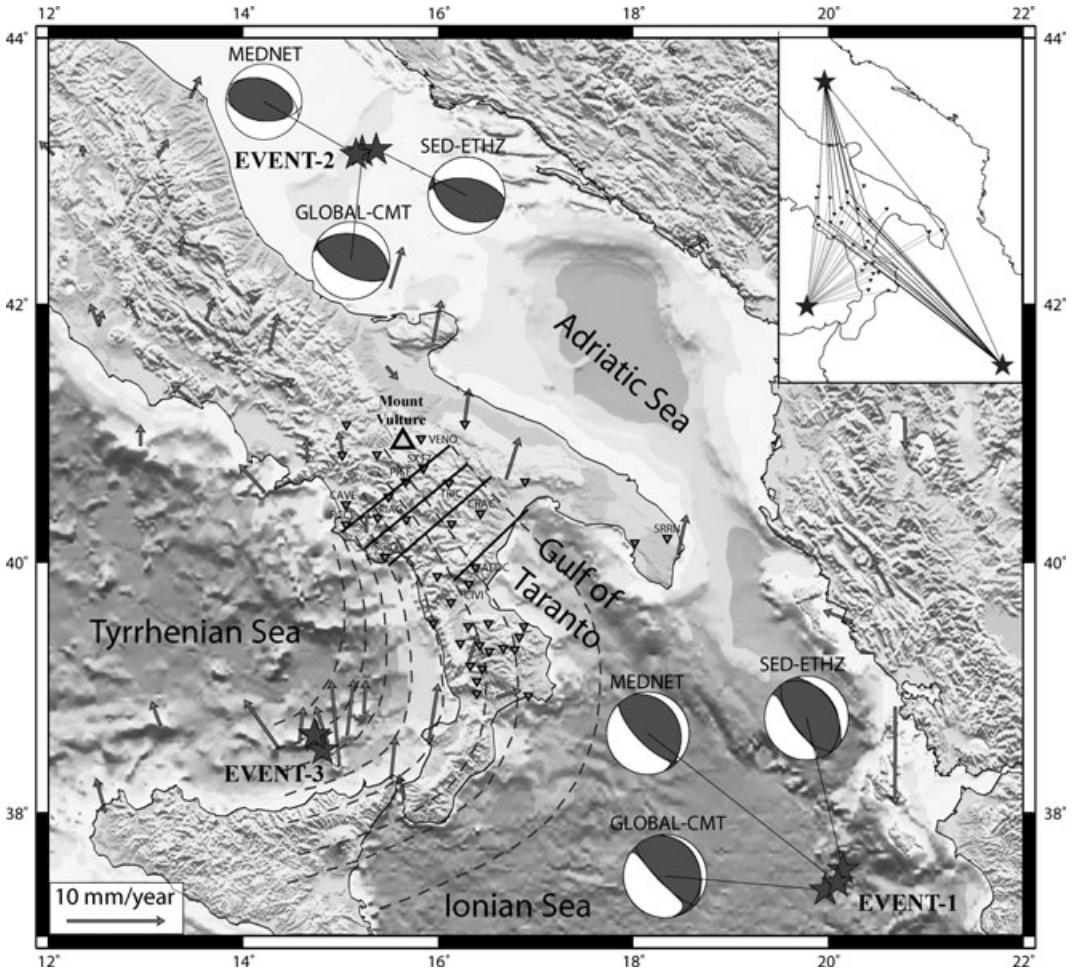

Figure 1. A topographic map containing the location of CAT/SCAN stations (triangles) and event locations (stars) of this study. Source mechanisms and locations reported by different institutions are as indicated. The map inset shows the corresponding ray paths. Dashed lines delineate the proposed slab depth at intervals of 50 km (Gudmundson & Sambridge 1998). Arrows show the GPS measurements of Serpelloni *et al.* (2006). The four parallel line segments indicate the surface trace of cross-sections to be presented in later figures.

Istituto Nazionale di Geofisica e Vulcanologia and the Università della Calabria. The dense network of ∼40 instruments operated between late 2003 and early 2005 offers an ideal laboratory to investigate the seismic structure. We analyse high-quality surface wave arrivals originating from two of the largest regional earthquakes during this period ($M_w = 5.7$; 2005 January 31 and $M_w = 5.3$; 2004 November 25). Through careful waveform matching we are able to resolve shear velocity and anisotropy down to ∼50-km depth and associate them with the tectonic history and dynamics of the southernmost Italian Peninsula.

2 DATA AND METHODOLOGY

2.1 Data and source parameters

We examine all regional earthquakes ($M_w \geq 4.8$) that took place within a 10° radius from the centre of the CAT/SCAN array. Selected events are then subjected to a surface-to-coda wave amplitude ratio test to ensure the robustness of the Love and Rayleigh waves for waveform modelling. Based on these criteria we retain three of the largest events (Table 1) in this region, most importantly events 1 and 2 that provide ideal source–receiver coverage in the southern Apennines, Apulia and Ionian Sea (Fig. 1, inset). We do not model the waveforms from event 3, mainly due to complications caused by a deep (238.9 km) source and short path lengths, but use the timing and amplitude information as an additional constraint on the resulting seismic structures from the first two events. The spatial resolution of the surface wave observations is largely dictated by the size of their Fresnel zones (Červený *et al.* 1984; Yomogida 1992, Fig. 2). The quarter-Fresnel zones reach the depths of ∼70 km and ∼45 km (see Fig. 2a) for the corresponding frequency bands of this study (low: 0.03–0.06 Hz; high: 0.05–0.2 Hz). In addition to frequency dependence, the depth sensitivity of the surface waves is also a function of polarization (Rayleigh versus Love). For instance, high frequency Love and Rayleigh waves have similar sensitivities to the top 20 km of the crust, but the sensitivity decays quickly for the SH-polarized waves at low frequencies (Fig. 2b). These frequency-dependent 'footprints' span 80–90 km laterally for individual source–station pairs at middle of the two frequency bands, which are considerably larger than those of receiver functions (e.g. 1.5–5 km at shallow depths, Steckler *et al.* 2008) but offer greater sensitivity away from the stations.

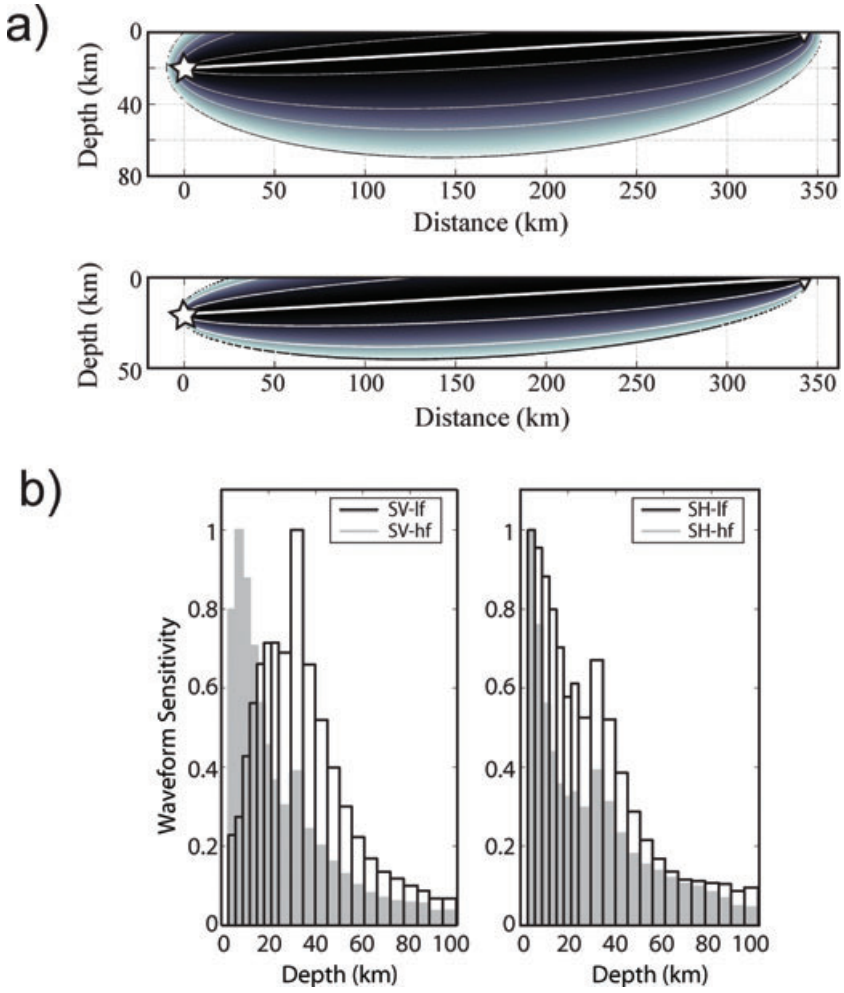

Figure 2. (a) Vertical cross-sections of Quarter Fresnel zones (Červený *et al.* 1984) at low (0.03–0.06 Hz, top panel) and high (0.05–0.20 Hz, bottom panel) frequencies. These wave 'footprints' are computed for event 1 (and station CAVE) assuming a single scatterer along the source–station path. For shallow earthquakes used in this study they can be reasonable proxies for surface wave Fresnel zones. (b) Depth sensitivities of vertically- (left-hand panel) and SH- (right-hand panel) polarized surface waves. These are estimated from the numerical derivatives of waveform misfit to the horizontally layered velocities (see eq. 1). The blank and the shaded histograms show the approximate sensitivities at low and high frequencies, respectively.

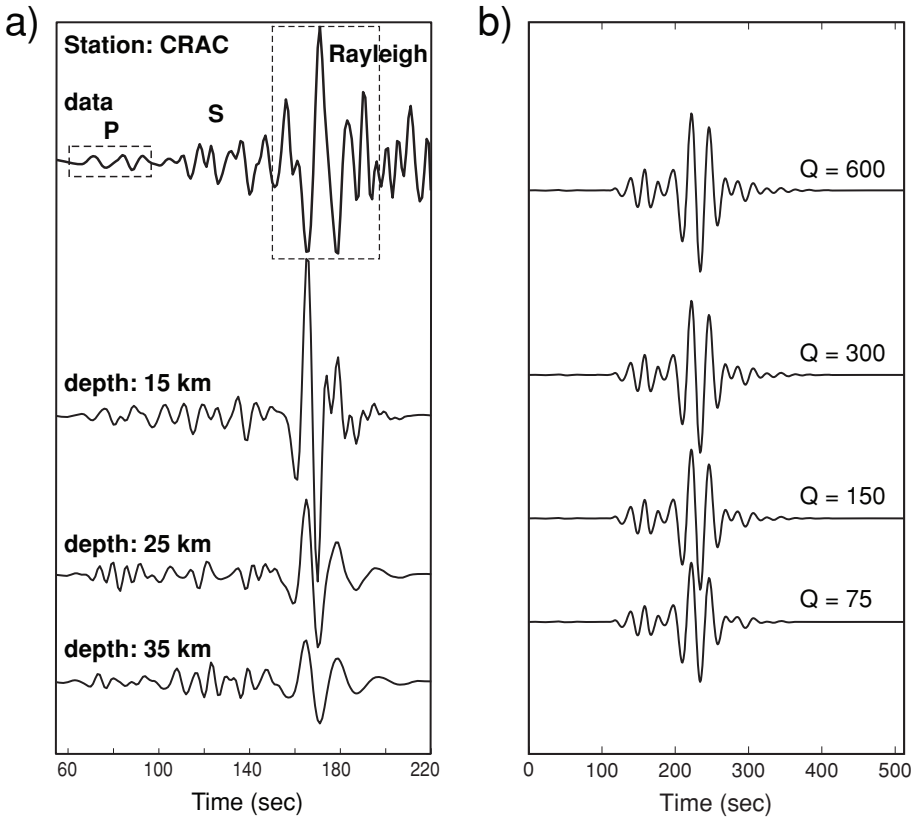

Figure 3. Waveform sensitivity to source depth and average Q structure. (a) Observed and predicted radial-component surface and body wave waveforms. The depth of event 1 is reported as 12 km (CMT solution), but the optimal solution (20 km) produces the best match to the observed body-to-surface wave ratio. (b) Sample Rayleigh wave waveforms computed based on different quality factors. In general, variations in Q structures have only modest effects on synthetic waveforms.

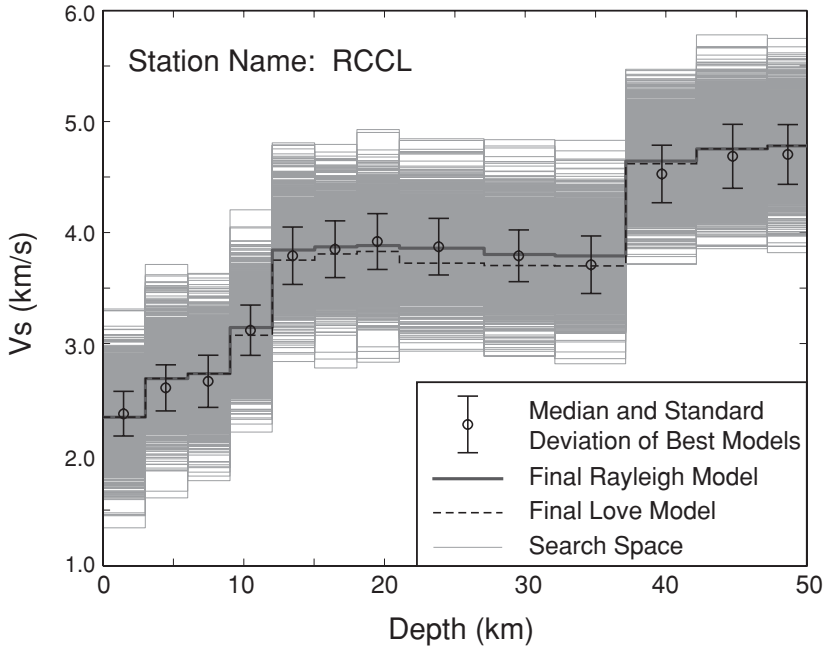

Figure 4. Model search space containing 2000 candidates for station RCCL. The errorbars and circles indicate the standard deviation and median of acceptable models, respectively. The thick grey (solid) line represents the best-fitting Rayleigh wave model, and the dashed line represents the final Love wave model. Both models fall within the errorbars.

We adopt the reported locations (latitude, longitude) and focal mechanism solutions from Global-CMT analysis (Dziewonski *et al.* 1981) to construct theoretical seismograms. The reverse faulting mechanisms from the CMT analysis are consistent with two regional body and surface wave solutions from Mednet-RCMT and SED-RMT (see Fig. 1). We compute waveforms using different hypocentre depths and seek the optimal match between the observed and predicted amplitude ratios of *P* and Rayleigh waves (*P*/*SV*) on the radial-component seismograms (Fig. 3a, Gu *et al.* 2005). This procedure is only weakly dependent on the starting velocity and *Q* models (Fig. 3b) as, for example, surface wave amplitude changes by less than 15 per cent for a wide range of average *Q*-values (75–600) in the top 50 km (see Fig. 3b). The optimal event depth based on the amplitude ratio approach is 20 ± 5 km for both events. Source effects associated with CMT, SED and Mednet solutions will be further discussed in Section 3.1.

2.2 Structure modelling

In this study, we simultaneously match the observed waveforms of Rayleigh and Love waves at two overlapping frequency bands (0.03–0.06 and 0.05–0.2 Hz). The synthetic seismograms are computed from the reflectivity method (Fuchs & Müller 1971; Kennett 1975, 1979, 1983; Kind 1976, 1978; Herrmann & Wang 1985) that carefully considers reflection and transmission of all possible waves originating from a buried point source in a horizontally stratified structure (Kennett 1983; Gu 2006). We fix the structure to PREM (Dziewonski & Anderson 1981) at depths greater than 50 km due to poorly observed long-period surface wave signals at frequencies below 0.025 Hz. We adopt the layer densities from PREM (Dziewonski & Anderson 1981) and the starting attenuation structure from a slightly modified *Q* model of Mele *et al.* (1996). The *P*-wave structure, which is allowed to vary in the modelling

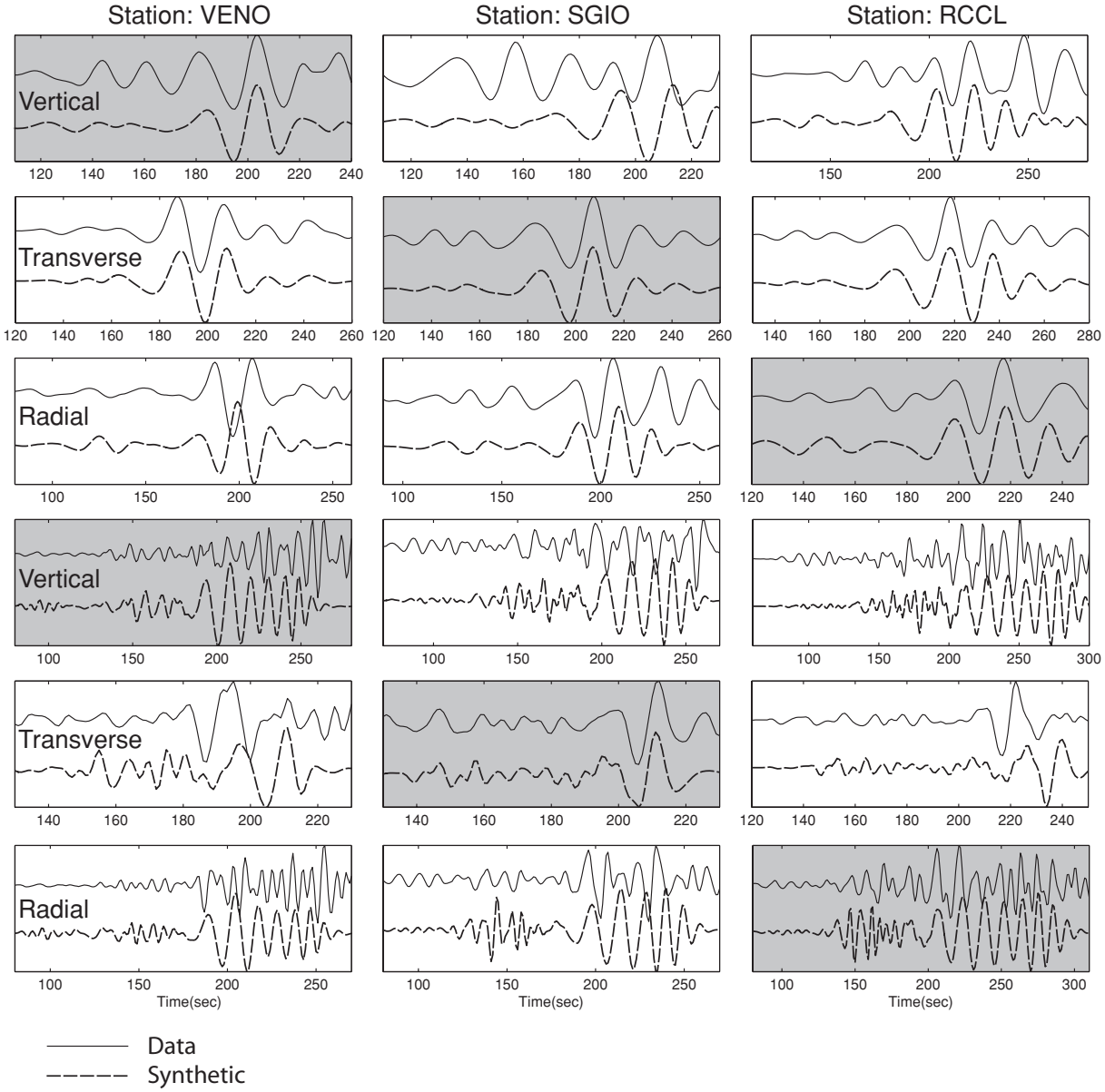

Figure 5. Sample surface wave waveforms from event 1. The data and synthetic seismograms are represented by solid and dashed lines, respectively. For each station, we determine the best-fitting model from the shaded component (two frequencies) and assess how well this model explains the two remaining (unshaded) components. The substantial misfit on the unshaded components suggests strong polarisation anisotropy.

procedure, is calculated by applying a scaling factor of 1.8 (Chiarabba *et al.* 2005) to the corresponding shear velocity for the same path; the dependence of surface waves on *P* velocity is negligible.

We explore a wide range of velocity values (randomly selected within 2000 models) for each layer to minimize potential biases associated with the choice of the starting shear velocity model. Using correlation coefficient as the objective function, we seek isotropic, path averaged shear velocity models that best match the observed Rayleigh and Love waves. All components and frequencies receive equal weights in the forward modelling process, and the median of candidate models with correlation coefficients greater than ∼0.7 (Fig. 4) is used as the starting model for a given source–station pair.

We introduce anisotropy to optimize the model fit to the observed Rayleigh and Love wave waveforms. To demonstrate the need for anisotropy along a given source–station path we compute three-component (vertical, radial and transverse) seismograms using the best-fitting model for the shaded component (Fig. 5). Substantial misfits, both in arrival time and in waveform characteristics, are apparent at stations VENO, SGIO and RCCL on the remaining two components (unshaded, see Fig. 5), suggesting both Love–Rayleigh (vertical Rayleigh versus Love) anisotropy and azimuthal (longitudinal Rayleigh versus Love) anisotropy.

We adopt both forward and inversion (Randall 1994) algorithms to improve the waveform fit at the two frequency bands of interest. A Monte Carlo method (Metropolis & Ulam 1949) is introduced to remove first-order timing and waveform differences between observed and model-synthetic seismograms, and the subsequent linearized waveform inversion (Randall 1994) 'fine-tunes' the model perturbations. In the latter approach, the partial derivative of a synthetic seismogram (S) with respect to the perturbed velocity (v) can be written in terms of a small perturbation in velocity (δv),

$$\frac{\partial S(t, v)}{\partial v} \approx \frac{S(t, v + \delta v) - S(t, v)}{\delta v}. \quad (1)$$

The sensitivity kernel for each model layer is computed numerically and forms a column of the Jacobian matrix in a weighted least-squares inversion (Randall 1994). Due to the nonlinear dependence of waveforms on layer velocities, this waveform inversion algorithm is most effective when velocity perturbations to the starting models are relatively minor; in this study the inverted perturbations do not exceed 3 per cent for most of the source–station pairs.

Finally, crustal thickness is interpreted from the best-fitting shear velocity models. The known trade-off between seismic velocity and Moho depth is effectively minimized by fitting the entire waveform instead of analysing dispersion or phase (Pasyanos & Walter 2002). In view of vertical model discretization (3 km in the top 24 km, 5 km from 24 to 60 km) the Moho depth uncertainty is no less than the minimum layer thickness of 3 km.

3 OVERVIEW OF STRUCTURE AND ANISOTROPY

3.1 Isotropic shear velocities

Figs 6 and 7 show examples of data and best-fitting model synthetic seismograms for events 1 and 2, respectively. The correlation coefficients generally exceed 0.8 for low frequencies and could reach

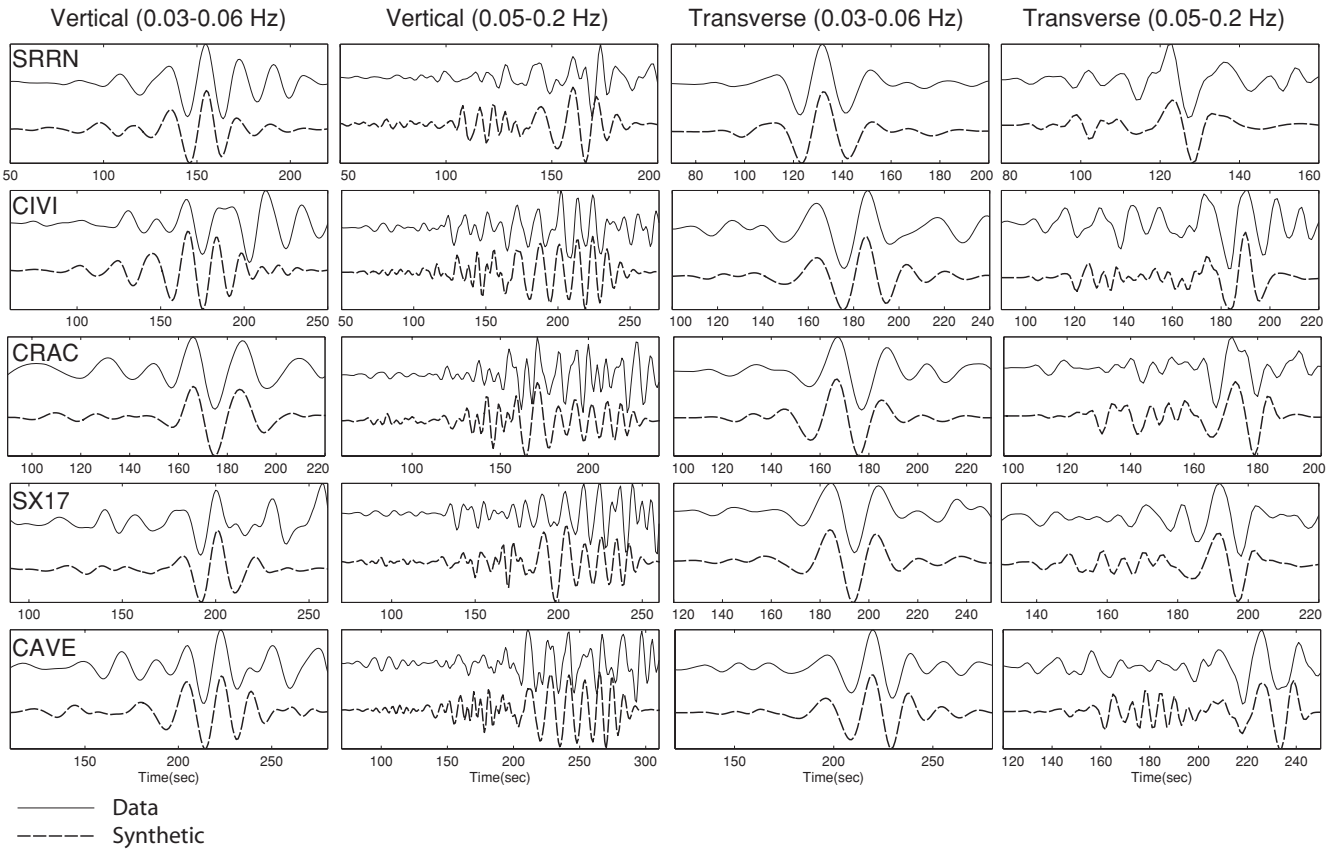

Figure 6. Vertical- and transverse-component waveforms of event 1 at low (0.03–0.06 Hz) and high (0.05–0.2 Hz) frequencies. The synthetic seismograms (dashed lines) and the observations (solid lines) are highly consistent for both frequency ranges.

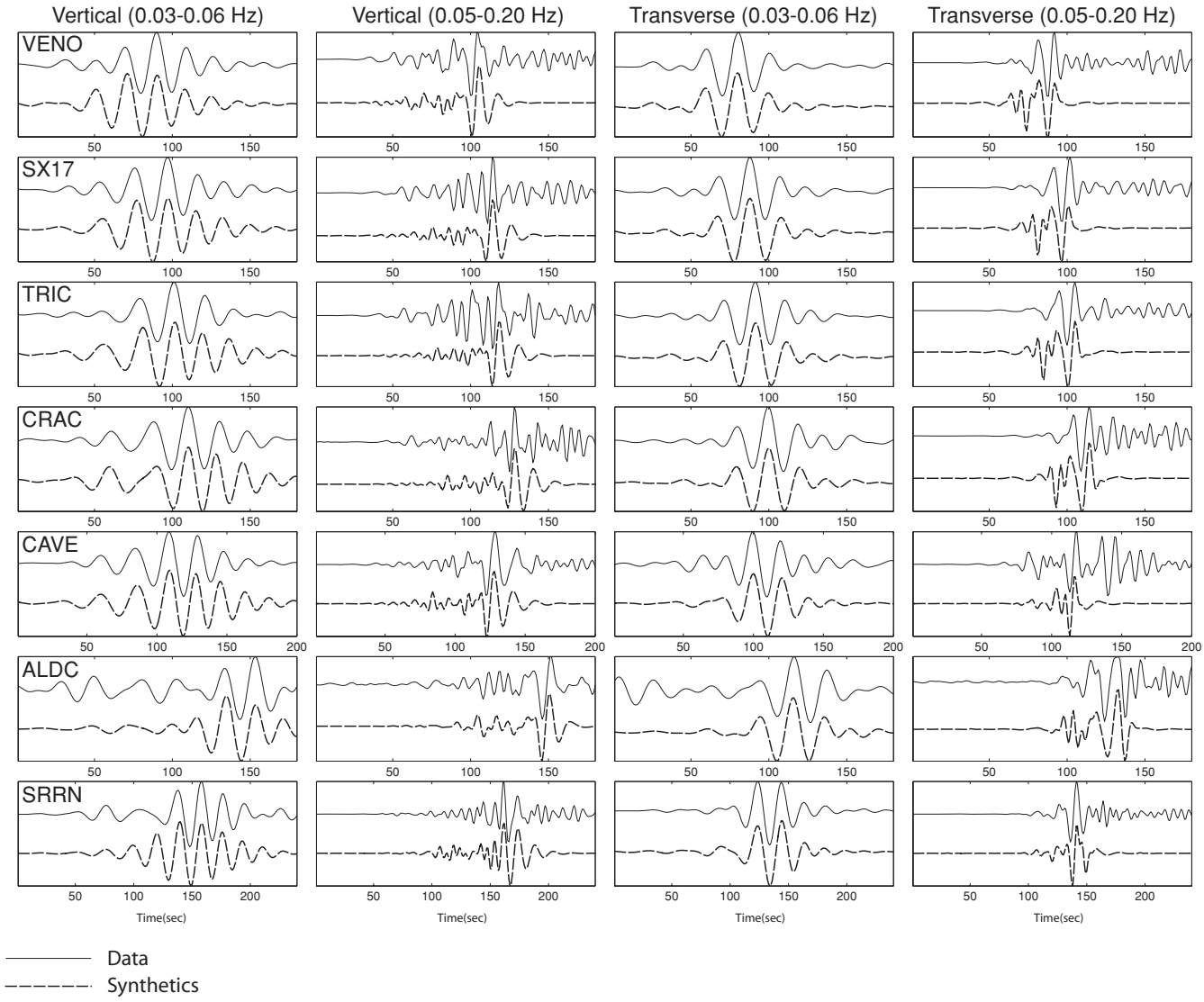

Figure 7. Vertical- and transverse-component recordings of event 2 at low (0.03–0.06 Hz) and high (0.05–0.2 Hz) frequencies.

as high as 0.85 for high frequencies. Both the main phase groups and the late-arriving reverberative energy are sufficiently explained by the best-fitting models at the vast majority of the stations. These waveforms are only weakly affected by the uncertainties in source location and mechanism (see Fig. 1): for example, the largest difference among the various reported location of event 1 is ∼20 km, which causes ∼5 per cent change in Love wave correlation coefficient and ∼2 s or less phase delay (Fig. 8). Such small-magnitude waveform and timing perturbations are indistinguishable from minor (<1 per cent) change in crust and shallow mantle shear velocities.

The best-fitting shear velocity models (Figs 9a and b) show peak-to-peak path-averaged speed variation of ∼2.5 km s^{-1} in the top 50 km. This range of perturbations is comparable to recent estimates from regional *P* waves (∼3 km s^{-1}; Chiarabba *et al.* 2005). For event 1, the lateral speed change of Love wave (∼0.6 km s^{-1} peak-to-peak) is considerably lower than that of Rayleigh waves (∼1 km s^{-1}). However, both wave types require a substantial velocity gradient in the depth range of 20–50 km. This feature is not present in models obtained from event 2 where velocity increases almost linearly with depth.

Spatial variations among the aforementioned 1-D models reflect the receiver-side structural differences due to ray path convergence near the source. To obtain an effective 3-D map of the study region we first compute the average 1-D structure from all source–receiver pairs. We then remove this mean structure from each path and place the resulting perturbations at the corresponding station location. As the final step, we interpolate between the stations using cubic polynomials to obtain a relatively crude approximation of the 3-D shear velocities. Fig. 10 shows a series of depth profiles across the Apenninic chain. Love and Rayleigh waves of event 1 records reveal a 20–25 km thick, low-velocity channel at depths below 24 km. This structure roughly follows the strike of the southern Apennines and attains its maximum depth near stations PICE and TRIC (Fig. 10c). The strength of the anomaly increases progressively towards the mountain belt as, for instance, the velocity at 30 km depth beneath station PICE is approximately 0.45 km s^{-1} slower than that under the coastal stations in the west. The low-velocity body gradually shallows towards the northwest and eventually merges with a modest low-velocity layer located in the shallow crust (6–12 km).

Recordings from event 2 offer further evidence for the tectonic divide between the Apennines (slow) and the Apulian Block (fast).

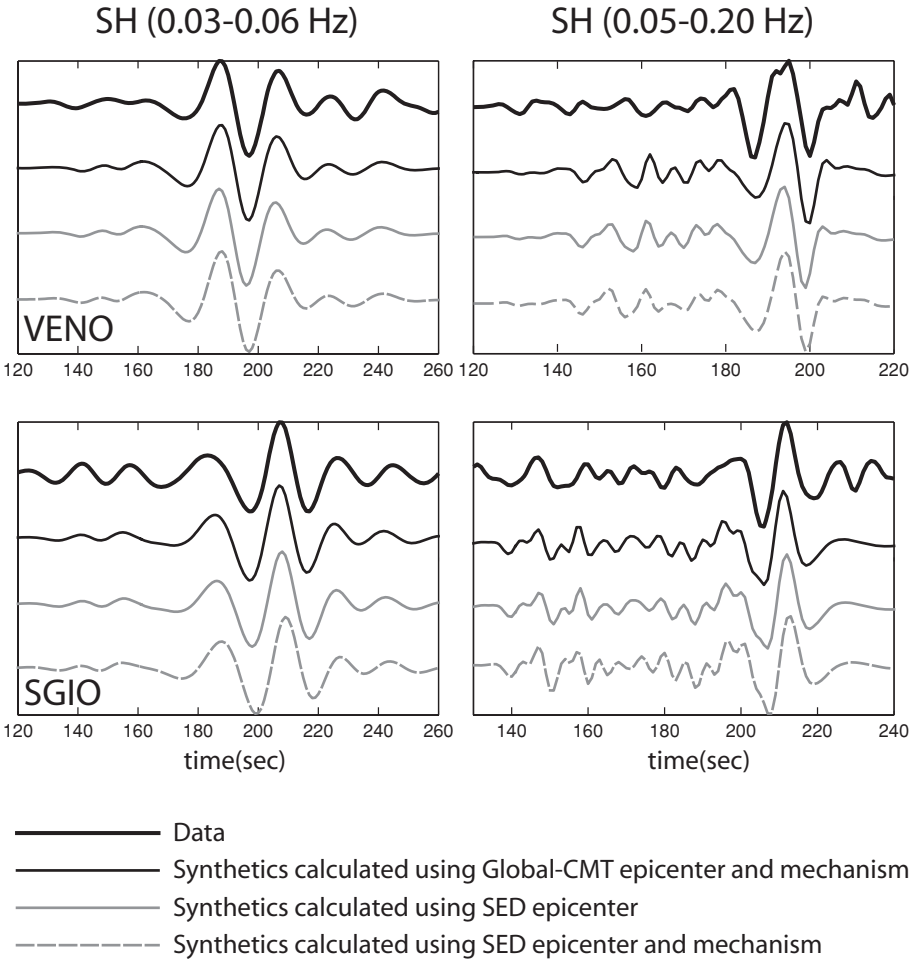

Figure 8. Effects of uncertain source location and mechanism on the transverse-component records of event 1. Observations (thick black lines) at both low (left-hand side) and high (right-hand side) frequencies can be well explained by a number of combinations involving Global-CMT and Swiss Earthquake Service (SED) source solutions.

Perturbations to the average structure (not shown) are similar to those obtained using event 1 records (see Fig. 10) and directly impact the arrival times of the surface waves. To verify the robustness the 3-D perturbations we order the stations according to the source–receiver path length within the southern Apennines, the slowest part of our study region (e.g. see Fig. 10), and generate predicted waveforms using the final models (one from each event) associated with station VENO. For event 2 (Fig. 11, left-hand panel), the timing misfit increases from <1 s for Love waves traversing the Apulian Block (e.g. at VENO, TRIC, CRAC and SX17) to $\sim$5 s for those that mainly sample the western flank of the Apenninc Chain (e.g. at CAVE and PIAG, Fig. 11, centre panel). Timing differences as large as 30 s for event 1 (Fig. 11, right-hand panel) are clearly visible between the western edge of the Apulian Block (at VENO) and the Apennines (e.g. at PIAG, CAVE, RCCL, SGIO, see Fig. 11, centre panel). The apparent correlation between delay time, path length and the waveform misfits are reflective of source–station orientation, distance and the geometry of the low-velocity body.

3.2 Low-velocity zone

The presence of a prominent low-velocity zone (at 25–40 km depth) and an overriding velocity increase (at 10–20 km depths) are best seen in the Rayleigh wave models (Fig. 9a). To illustrate the importance of these features in matching surface wave phase velocities and amplitudes, we perturb the model layers from 10 to 70 km (Fig. 12a) and compare the resulting predicted waveforms with the observations. In general, the characteristics of velocity gradients at shallow crustal depths (Models 1 and 2, Fig. 12a) play an important role in producing the late-arriving, reverberative Rayleigh waves at high frequencies (Fig. 12b), whereas a lower-crustal/upper-mantle gradient (at $\sim$40 km, Models 3 and 4, Fig. 12a) is highly sensitive to the amplitude ratios between the first surface wave arrival and the subsequent peaks at low frequencies (see Fig. 12b). Significant deviations of either gradient from our best-fitting models (solid line, Fig. 12a) severely degrade the correlation between the observed and model-predicted waveforms.

It is worth noting that although the waveforms presented thus far have been strictly limited to two overlapping frequency windows, the observed station records are generally well matched by model synthetics over much wider frequency bands (Fig. 13). Source–station pairs away from the low-velocity zone (event 1-to-SRRN; Fig. 13a) are generally characterized by short wave trains and increasing speeds at long periods. In contrast, surface waves propagating towards stations on the Apenninic foreland (e.g. TRIC) are strongly affected by the underlying low-velocity zone and exhibit constant phase delays at periods longer than $\sim$25 s (Fig. 13b). These

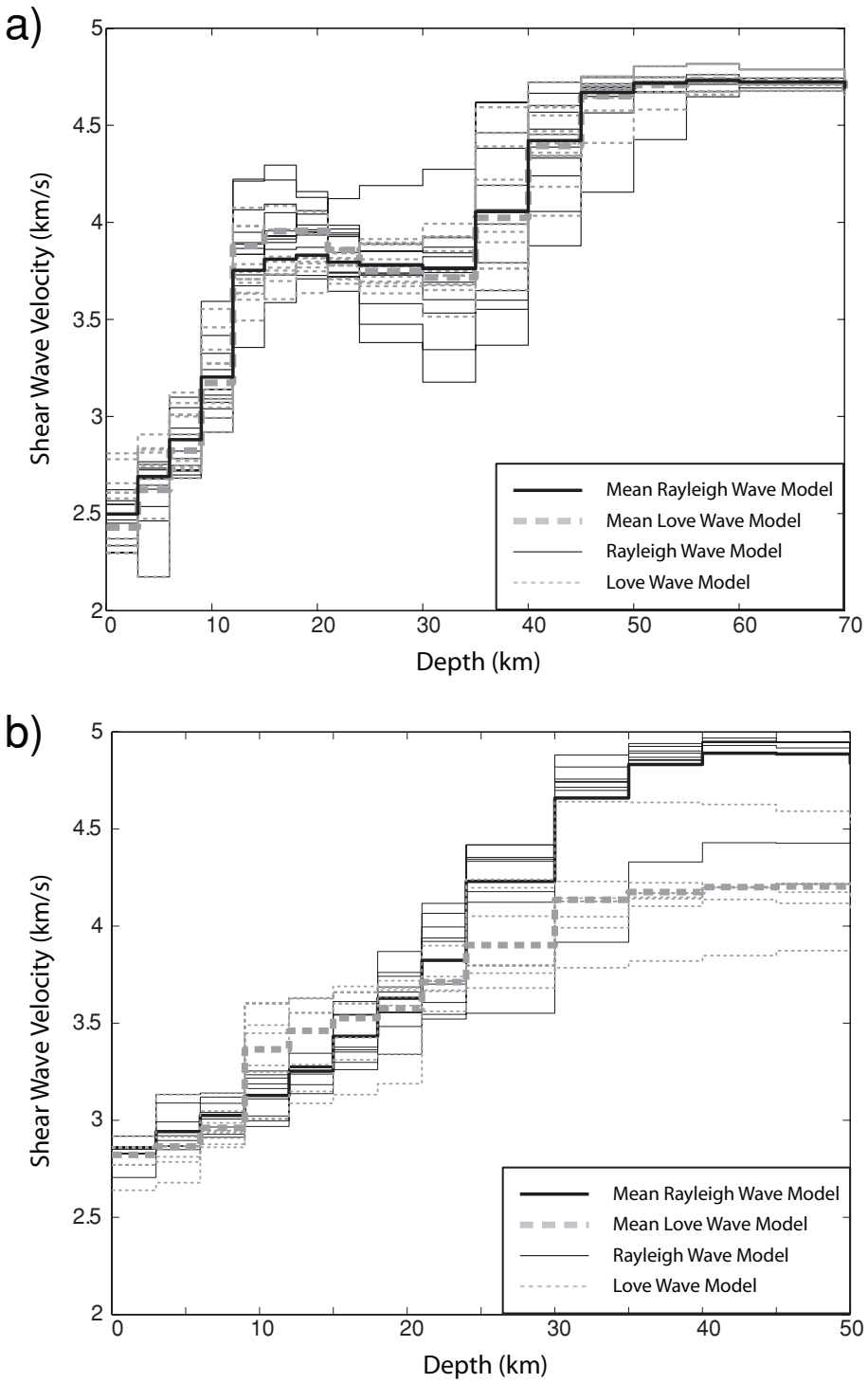

Figure 9. Seismic velocities determined from Rayleigh (thin solid lines) and Love (thin dashed lines) waves from all stations. (a) Final shear velocity models from event 1 records. The average Rayleigh and Love wave models are highlighted by the thick solid and dashed lines, respectively. Most of the event 1 models show a low-velocity layer below 20 km. (b) Models determined from event 2 data. Velocities increase linearly with depth. The main model difference between event 1 (panel a) and event 2 (panel b) paths reflect the average structural difference between the Adriatic and Ionian Sea regions.

anomalous dispersion curves are accompanied by high-amplitude coda waves on the vertical-component seismogram of TRIC and, to lesser degrees, of PICE and SX17 (see circled waveforms in Fig. 13b). These energetic coda waves are poorly explained by the simplistic 1-D waveform simulations (see Fig. 13b) and their nature of the coda waves is unclear, though body or surface waves scattered off a complex 3-D low-velocity volume (see Fig. 10) could be partly responsible. Strong anisotropy (see Section 3.4) beneath the Apennines may also give rise to quasi-Rayleigh waves (Silver 1996; Levin *et al.* 2007) that, depending on the strength and the orientations of the anisotropic structure, could affect the early portions of the coda wave window. The origin of the persistent

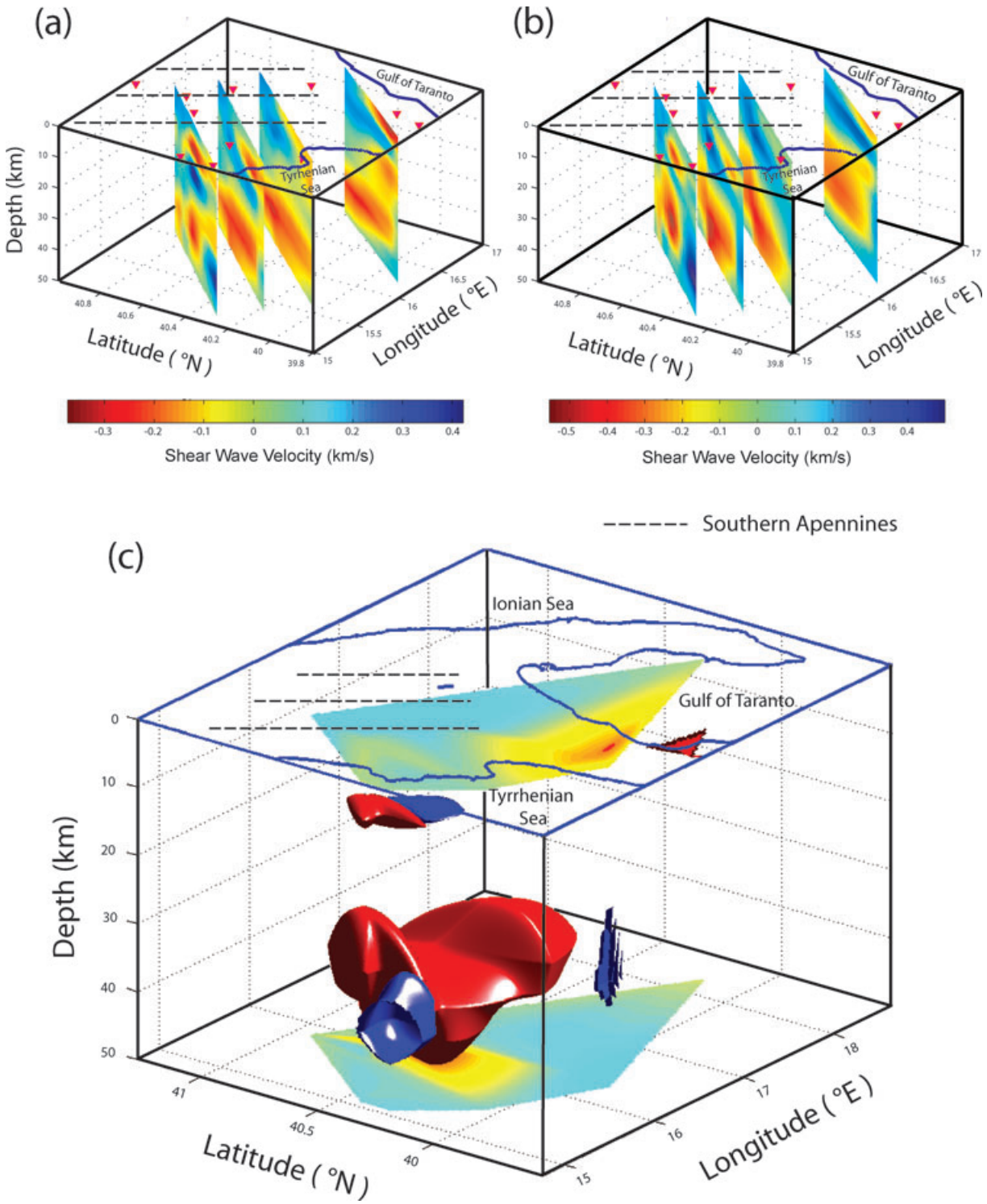

Figure 10. Cross-sections of Love (a) and vertically polarized Rayleigh (b) wave models obtained using event 1 recordings. The surface projections of the cross-sections are approximately perpendicular to the Apenninic chain (see Fig. 1). The presence of a laterally coherent, deep crustal low-velocity layer is observed beneath the Apennines. A shallow crustal low-velocity layer is also visible in the northern parts of the study region. (c) An isosurface (threshold = 0.3 km s^{-1}) map of the Rayleigh wave models beneath the study region. An anomaly resembling a 'horse saddle' is observed beneath the southern Apennines. This anomaly orients in the SE–NW direction and potentially extends to depths below 50 km in the central part of the southern Apennines.

vertical-component energy 150–200 s after the fundamental-mode surface waves remains enigmatic. Recent observations and simulations of surface waves reflected off the crustal root beneath the northern Apennines (e.g. Stich & Morelli 2007) present an interesting possibility. The suggested frequency band for the reflected surface waves (15–20 s periods; Stich & Morelli 2007) is also consistent with that shown in Fig. 13(b). However, for a reflected surface wave to be a viable explanation in the southern Apennines, the

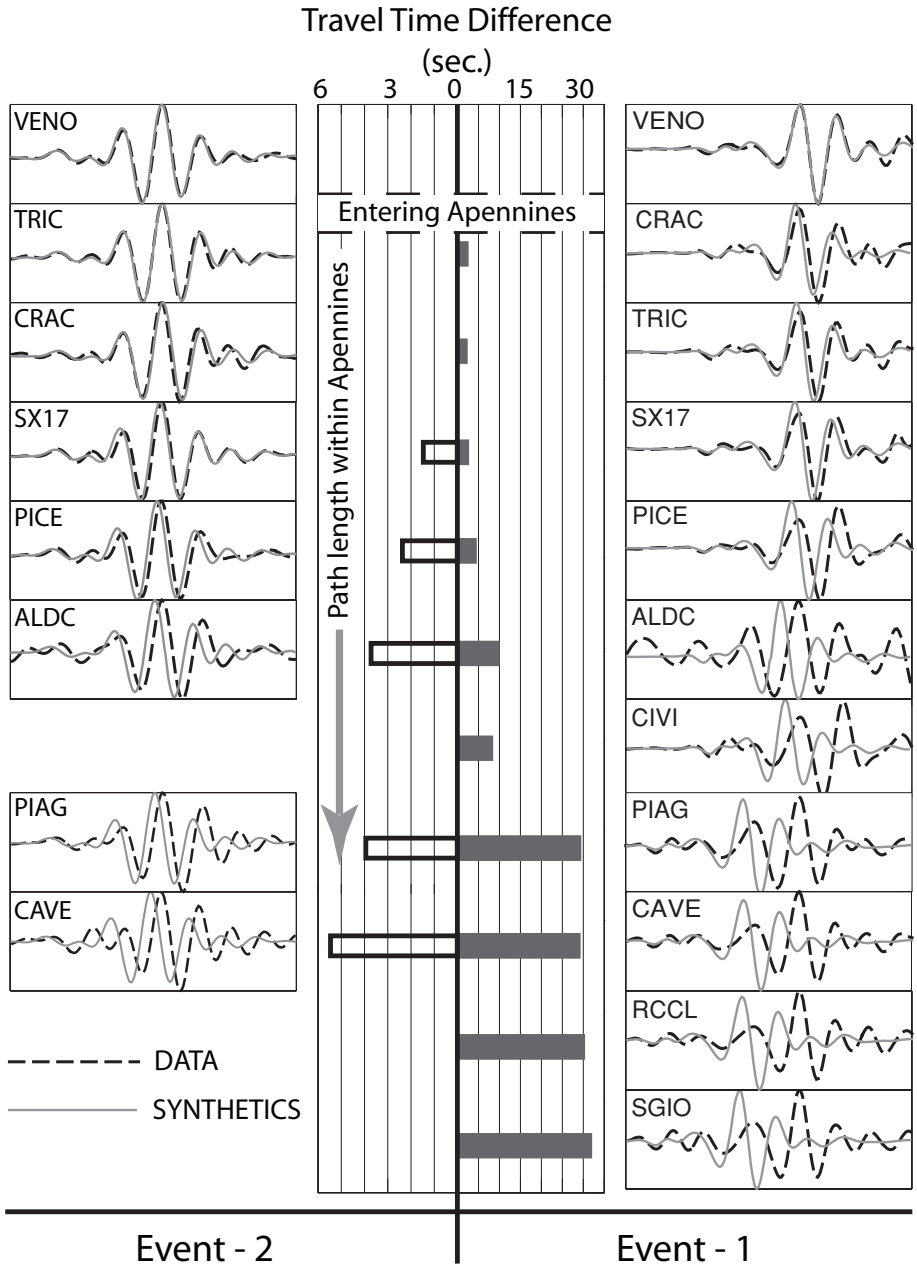

Figure 11. Low frequency (0.03–0.06 Hz) SH waves (dashed black line) from event 1 (right-hand panel) and event 2 (left-hand panel) recorded by all available CAT/SCAN stations. All synthetic seismograms (solid grey line) are calculated using the best-fitting models (one from each event) for station VENO, located in Bradanic foredeep. For both events Love waves propagating near the western flanks of the southern Apennines suffer major delays. This is evidenced by the rapidly growing traveltime misfit (middle panel) at stations closer to the reported low-velocity channel.

reflector should (1) reside in the north–northwest of the seismic array at a distance of 300–500 km and (2) be able to focus the surface wave and channel it preferentially towards the Apenninic stations. The two aforementioned conditions are necessary to account for large delay times and amplitudes of the coda waves, respectively. A future study of 3-D wave propagation will be needed to confirm the nature of coda waves presented in Fig. 13(b).

Waveforms from event 3 (Fig. 14) offer supporting evidence for a low-velocity zone beneath the southern Apennines. Rayleigh waves that are sensitive to Regions 2 and 3 experience major time delays and amplitude reductions relative to those propagating in the Calabrian and Apulian Blocks. The relative path differences reveal that the boundaries between these three tectonic regimes (see Figs 9a and 10c) are relatively sharp.

3.3 Crustal thickness

The observed low-velocity anomaly may be interpreted as crustal, assuming the modest increase in seismic speed beneath it (see Fig. 9a) represents the Moho interface. Fig. 15 shows the isosurfaces of the low- velocity zone (white) and a subjective mantle shear velocity of 4.0 km s^{-1} (black) beneath the study area. The Moho depths on the eastern and western flanks of the Apennines are identified at ∼38 and 32 km, respectively, whereas station TRIC west

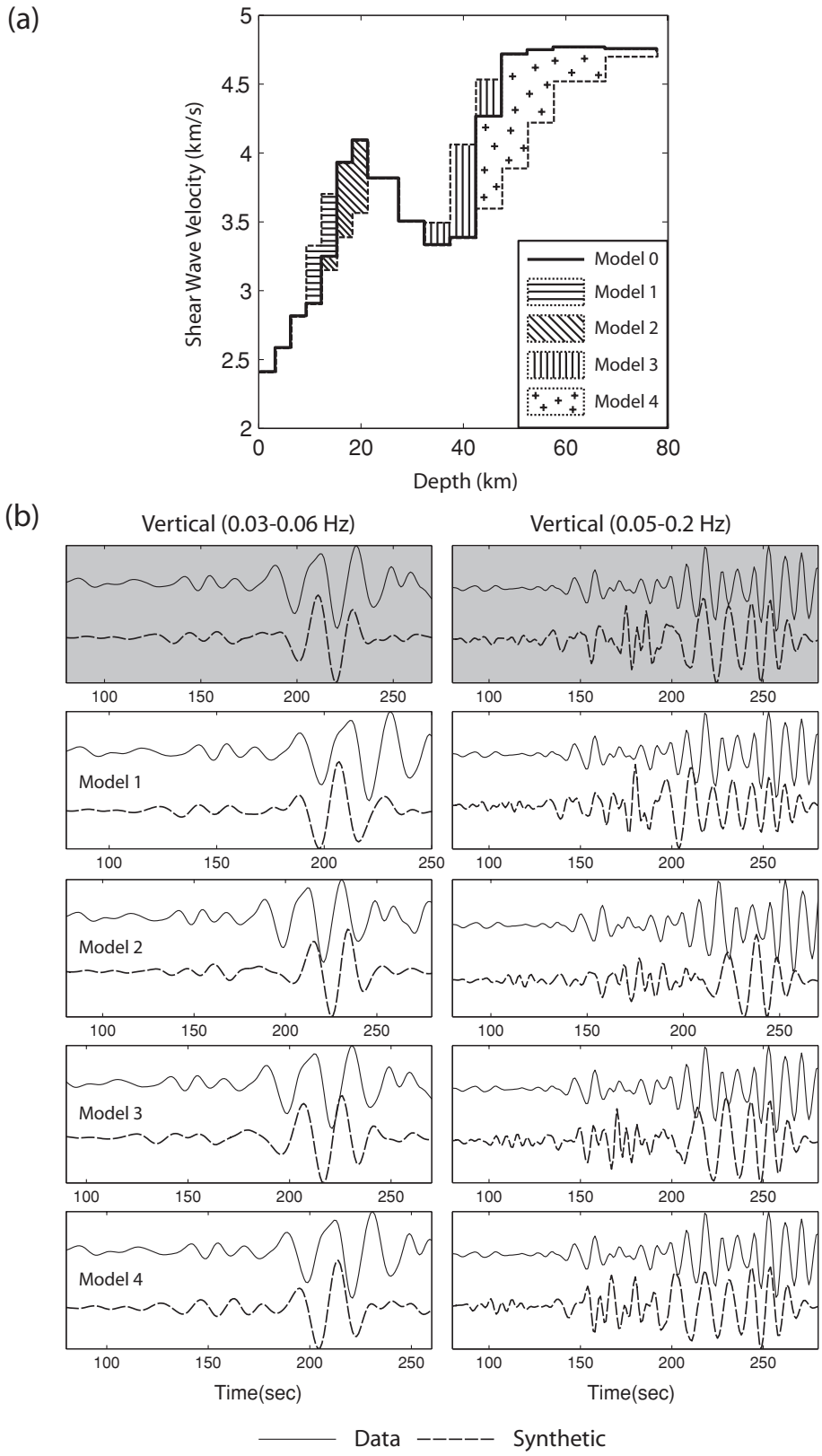

Figure 12. Sensitivity of vertical-component waveforms at station PICE to major crustal and upper-mantle velocity gradients. (a) Five different 1-D models used in the calculation of synthetic waveforms. Model 0 (black line) is the eventual best-fitting model beneath station PICE. (b) High- and low-frequency Rayleigh waves are shown by the right- and left-hand columns, respectively. In both cases, data and waveforms computed based on the best-fitting model (Model 0 of Fig. 12a) are shaded and well matched. Waveform predictions from models containing different velocity gradients in the lower crust and upper mantle (see Fig. 12a) do not match the observed phase velocities and/or waveform characteristics. A well-constrained low-velocity zone is critical in reproducing the high-frequency reverberations after 220 s.

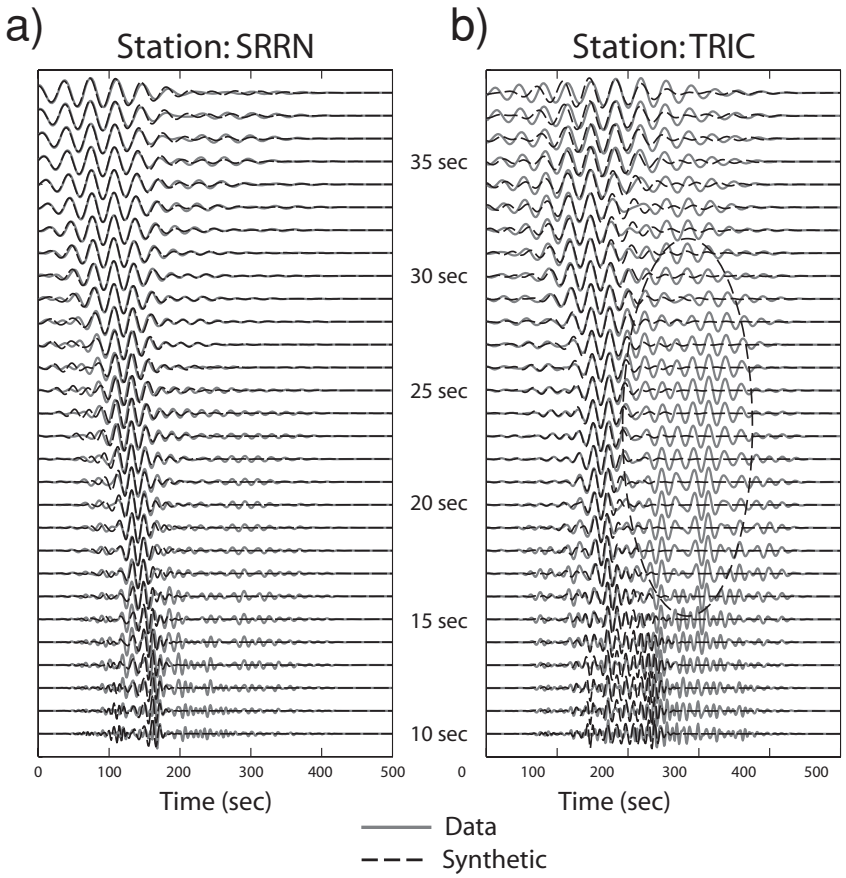

Figure 13. Sample vertical-component waveforms (event 1) showing the effect of surface wave dispersion. The numbers on the *y*-axis denote the centre frequencies of 10-s wide bandpass filters. The data after filtering are shown by the solid grey lines and the corresponding synthetic seismograms are shown by the dashed lines (black colour). The circled waveforms of station TRIC are poorly explained by our 1-D synthetic seismograms.

of the Bradanic foredeep is underlain by a deep crust bottoming at ∼45 km depth. The seismic jump (<7 per cent) at the presumed Moho interface is much smaller than the global averages of 11 per cent in PREM (Dziewonski & Anderson 1981) and 16 per cent in IASPEI91 (Kennett 1991). A reference mantle velocity value of 4.2 km s^{-1} shifts the Moho interface down by 3–5 km, but it will not significantly impact the velocity contrast between the lower crust and upper mantle.

3.4 Love and Rayleigh wave anisotropy

We compute model differences between vertically polarized Rayleigh waves and SH-polarized Love waves as an approximation for the extent of anisotropy beneath the study region. These model differences do not represent radial anisotropy (or transverse isotropy) due to the presence of significant azimuthal anisotropy (see Section 3.5). For each station, we calculate a percentage anisotropy based on model difference (vertical Rayleigh–Love) and the Voigt average (Voigt 1928) of these two types of models. Fig. 16 shows the spatial variation of Love–Rayleigh anisotropy along the southern Apenninic chain: significant anisotropy with positive SV–SH values is present at shallow crustal depths beneath most stations. These positive model differences appear to weaken and deepen towards the western flank of the Apennines (Fig. 16a). The strongest anisotropy exists at 20–40 km depth, where shear velocities obtained using SH-polarized waves far exceed those from vertical, SV-polarized waves. The shape of this anisotropic body is delineated by isosurfaces of anisotropy values below –5 per cent (Fig. 16b). Its orientation roughly follows a 10° angle towards the east of the southern Apennines. The deepest part of this anisotropic structure is found beneath station TRIC, coinciding with the aforementioned low-velocity zone at 30–50 km (see Fig. 10). Anisotropy of such magnitude could cause the Love waves to travel up to 14 per cent faster than the vertical Rayleigh waves for a given source–station pair, in addition to the expected traveltime difference associated with the distinct nature of these two wave types.

3.5 Azimuthal anisotropy

The dimension and characteristics of crustal anomalies are further constrained by azimuthal anisotropy, a polarization asymmetry that we estimate from the phase delay of theoretical Rayleigh waves (assuming the best-fitting vertical Rayleigh model) on the radial-component seismograms. The inset of Fig. 17(b) shows the average traveltime residuals of the Love-wave models and the orientation of the symbols indicate the faster polarization direction. In general, radial-component Rayleigh waves propagate at significantly slower speeds than the vertical-component Rayleigh waves, whereas models derived from both components are, on average, slower than those from Love waves (transverse component). Azimuthal anisotropy is especially prominent beneath stations PICE, TRIC, CRAC, SX17, CIVI—all appear to be underlain by strong low-velocity and anisotropic layers below 25 km. The strength and fast direction of wave propagation/polarization are roughly

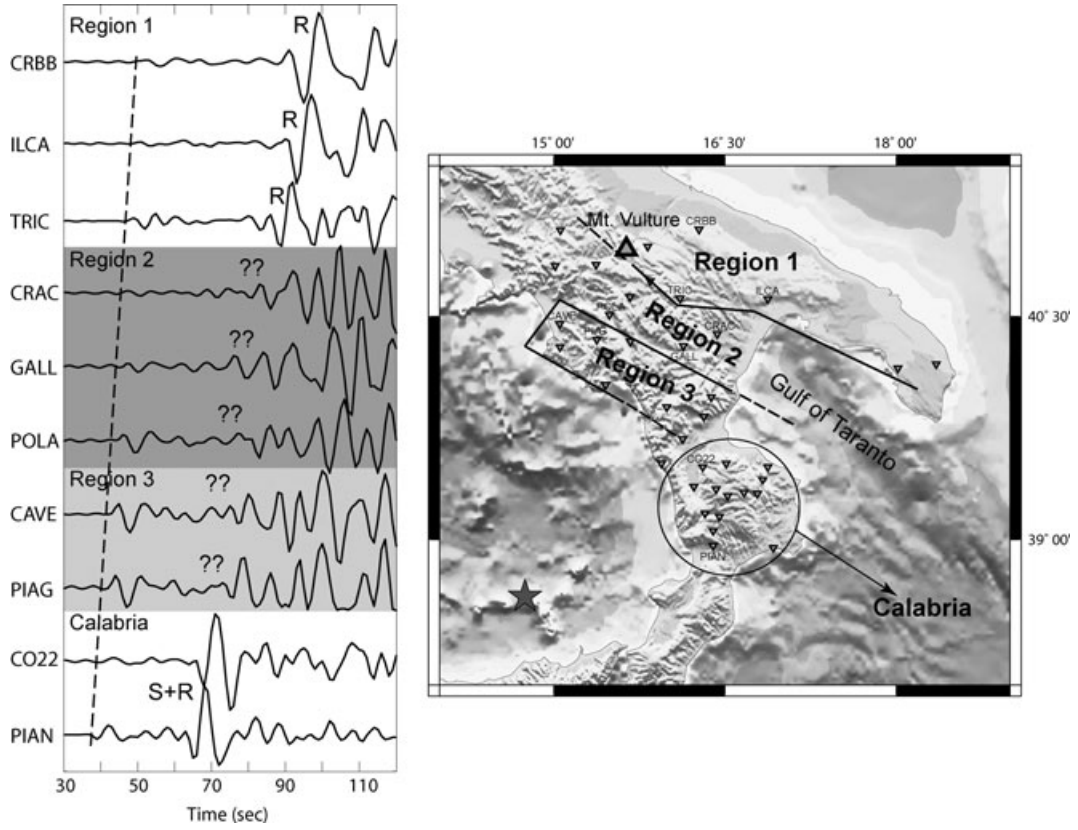

Figure 14. High-frequency (0.05–0.2 Hz), vertical-component waveforms from event 3 suggest three (possibly four) major tectonic blocks. Stations within the Calabrian and Apulian Blocks (Region 1) show relatively simple waveforms containing a strong Rayleigh arrival. The same phase (marked by ??, left-hand panel) are strongly attenuated and delayed within Region 2, within which a major low-velocity zone is identified (see Figs 9a and 10). The southeastern (in Gulf Taranto) and northwestern (near Mt Vulture) borders of this low-velocity zone (right-hand panel) are unclear due to the lack of station coverage.

consistent with those of Pn waves (see Fig. 17c; Mele *et al.* 1998), and the amount of anisotropy (of both azimuthal and potentially 3-D in nature) decreases considerably west of the Apennines. The dominant fast directions of wave propagation near the Tyrrhenian coast are roughly vertical (not shown).

It is worth noting that our preferred fast directions are only a crude approximation for the anisotropic structure in the study region. Since the orientation of three-perpendicular components (radial, transverse and vertical) is pre-determined by the source and station locations, the theoretical uncertainty could be as large as 45° at a given station due to limited azimuth coverage. Nonetheless, a northeast–southwest fast direction is supported by Pn observations and the present-day plate motions beneath the Apennines.

4 DISCUSSION AND INTERPRETATION

Since the termination of southwestward subduction of the Adriatic plate, the formerly dominant compressional forces have been gradually replaced by NE–SW extensional forces (Hippolyte *et al.* 1994). The presence of local extensional regimes, coupled with ongoing plate convergence beneath the central/northern Apennines and the Calabrian Arc, are conducive to asthenospheric upwelling beneath the southern Apennines. In fact, there has been ample evidence of low-velocity layers in the shallow mantle beneath the Apennines (Wortel & Spakman 1992, 2000; Amato *et al.* 1993; Piromallo & Morelli 1997, 2003; Lucente *et al.* 1999; Cimini & De Gori 2001; Panza *et al.* 2003; Spakman & Wortel 2004), prompting a suite of dynamic models characterized by lithospheric delamination, detachment, tear or slab window(s). For example, a lithospheric delamination process was invoked by Mele *et al.* (1996, 1997) to explain the high attenuation of Sn wave propagation beneath the southern Apennines. At slightly greater depths (∼100 km), slab detachment/tear hypotheses provide viable mechanisms for the upward intrusion of hot asthenospheric material (Wortel & Spakman 1992, 2000; Piromallo & Morelli 1997, 2003; Cimini & De Gori 2001; Panza *et al.* 2003; Spakman & Wortel 2004). A slab window (Amato *et al.* 1993) between the central Apennines and Calabria, or subduction of a possible continental promontory (Lucente *et al.* 1999), could also account for the excess of heat and/or partial melt below the southern Apennines. The likely presence of a low-velocity mantle regime has been complemented by reports of low-velocity (and low density) crustal regimes beneath the study region. For example, a negative Bouguer gravity anomaly was identified beneath the Apennic chain (Tiberti *et al.* 2005), which may be caused by the presence of hot and molten asthenospheric material (D'Agostino & McKenzie 1999). The existence of such a low-velocity crustal body is supported by recent results of regional seismic surveys and heat-flow modelling (Di Stefano *et al.* 1999; Cimini & Gori 2001; Chiarabba *et al.* 2005; Solaro *et al.* 2007; Steckler *et al.* 2008).

Our surface wave analysis presented here provides first-order constraints on the shape, depth and anisotropic nature of the low-velocity body at lower-crust/upper-mantle depths beneath the southern Apennines. The low-velocity zone is significantly shallower than the proposed depth of partial melting (at 100+ km) in the dynamic models of the region. The location of the anomaly coincides with a low-velocity channel spanning the entire Apenninic chain

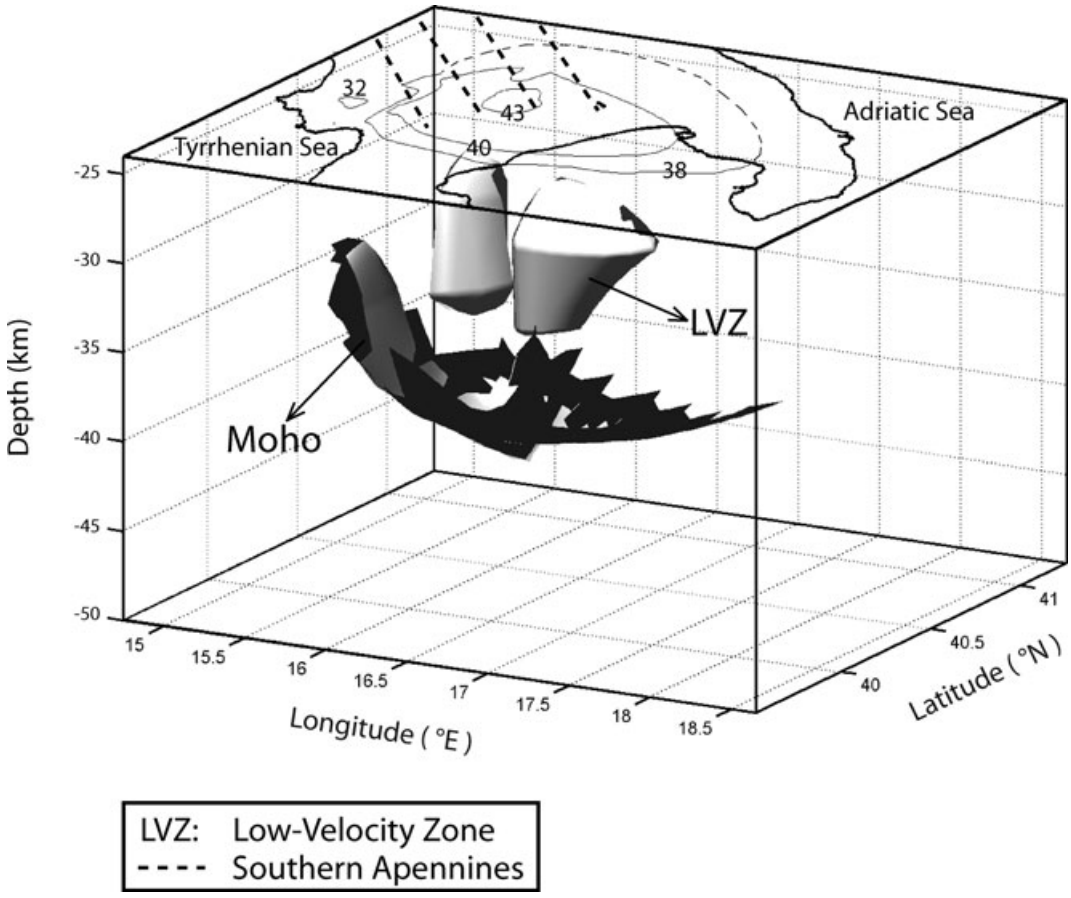

Figure 15. Isosurfaces of 3.5 and 4.0 km s^{-1} model speeds are shown by light and dark grey colours, respectively. The depth of the Moho interface (contour lines) is projected onto the top surface. Crust appears to thicken by 7–10 km beneath the southern Apenninic chain.

(Di Stefano *et al.* 1999; Cimini & Gori 2001), with the high attenuation zone inferred from the absence of Sn waves and slow Pn waves (Mele *et al.* 1996, 1997, 1998), as well as with existence of the complex reverberative energy reported by a recent receiver function study using the same data set (figs DR.3.7. and DR.3.9.; Steckler *et al.* 2008). Figs 17(a), (b) and (d) compare the result of our study with those from *P*-wave tomography (Cimini & Gori 2001) at 40 km depth. The spatial resolution of the coherent, low-velocity anomaly is considerably higher than peninsula-wide anomalies from earlier cell-based dispersion analyses (Pentevivo & Panza 2002; Panza *et al.* 2003; Venisti *et al.* 2005). Furthermore, the surface waves used here have greater depth sensitivity to structural contrasts along the NE–SW cross-section through the study region, as evidenced by PICE (slow) and VENO (fast).

Our analysis of shear wave anisotropy imposes additional constraints on the characteristics and origin of the low-velocity zone. The sensitivity of the surface wave frequencies (see Fig. 16) suggests that anisotropy could be as large as 14 per cent within the crust, which is too large to be explained by the alignment of mantle minerals such as olivine even if asthenospheric material is present (as proposed by earlier studies). In other words, flow-induced shear dislocation (Margheriti *et al.* 2003; Civello & Margheriti 2004; Baccheschi *et al.* 2007) is unlikely the main source of Love–Rayleigh and azimuthal anisotropy beneath the southern Apennines. A careful examination of the ray paths relative to the orientation/dimension of the observed low-velocity anomaly reveals strong shape-induced anisotropy. On average, ray paths that sample the eastern flanks of the Apennines are mostly embedded within an elongated low-velocity body, resulting in major reduction in radial-component Rayleigh wave speed. Such path effect is less severe for Love waves (transverse component), as the large Fresnel zone size (roughly 200 km for a 20 s wave; Zhou *et al.* 2006) enables these transversely polarized waves to sample the 'normal' crust outside of the relatively narrow low-velocity regime. The resulting model difference could be sufficient to explain the observed, NE–SW oriented azimuthal anisotropy. In addition, the overall anisotropy decreases further west as the rays intersect the low-velocity structure at oblique angles. In these cases, the orientation and strength of anisotropy are dictated by the path length within the low-velocity body, by the aspect ratio of the structure, as well as by their relation to the particle motion/wavelengths of the surface waves.

The vertical extent of the anisotropic, low-velocity anomaly remains poorly resolved considering the limited frequency band (hence, depth) of the surface waves in our analysis. The depth of the Moho, that is believed to separate a mafic crust from an ultramafic asthenosphere under the southern Apennine region, is equally debatable. In the absence of major seismic jumps associated with average crust and mantle interface (see Fig. 9a), our observation of a locally thickened crust beneath the southern Apennines (see Fig. 15) is consistent with earlier reports in this region (Meissner *et al.* 1987; Di Stefano *et al.* 1999; Menardi Noguera & Rea 2000; Dèsez & Ziegler 2002; Marone *et al.* 2003; Chiarabba *et al.* 2005; Scrocca *et al.* 2005). Most of these studies show near-average crustal thicknesses ranging from 25 to 35 km beneath the Apulian foreland and

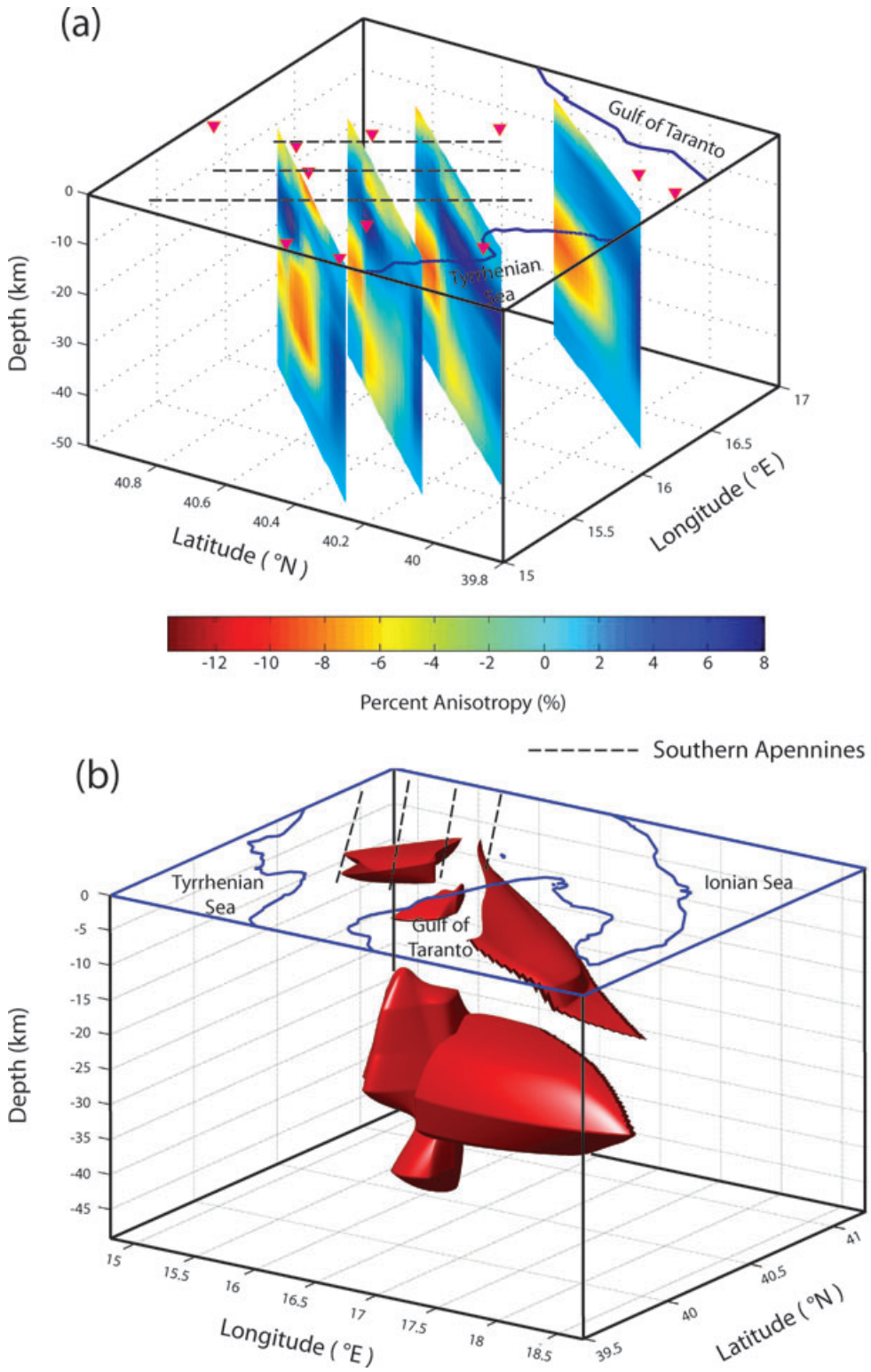

Figure 16. (a) Cross-sections of percent anisotropy relative to the isotropic velocities. Blue colours represent regions where vertically polarized Rayleigh waves travel faster than Love waves. (b) A 5 per cent isosurface of Love–Rayleigh anisotropy. The main anisotropic pattern appears to be narrow, elongated and reasonably thick. The negative (Rayleigh < Love) velocity anomaly (see Fig. 10) roughly follows the strike of the southern Apenninic chain.

the Tyrrhenian-sea side of the Apennines, while the crust beneath the centre of the southern Apenninic chain could be as thick as 45–50 km (Raykova & Nikolova 2007). Our estimated Moho depths are within 2–3 km of the reported values in Raykova & Nikolova (2007) based on surface wave dispersion, and are ∼8 km deeper than those of Steckler *et al.* (2008) based on receiver functions from the same CAT/SCAN database.

Qualitatively, an increase in lower-crustal speed or a decrease in upper-mantle speed could both reduce the seismic jump at the base of the crust. The former requires the lower crust to be more

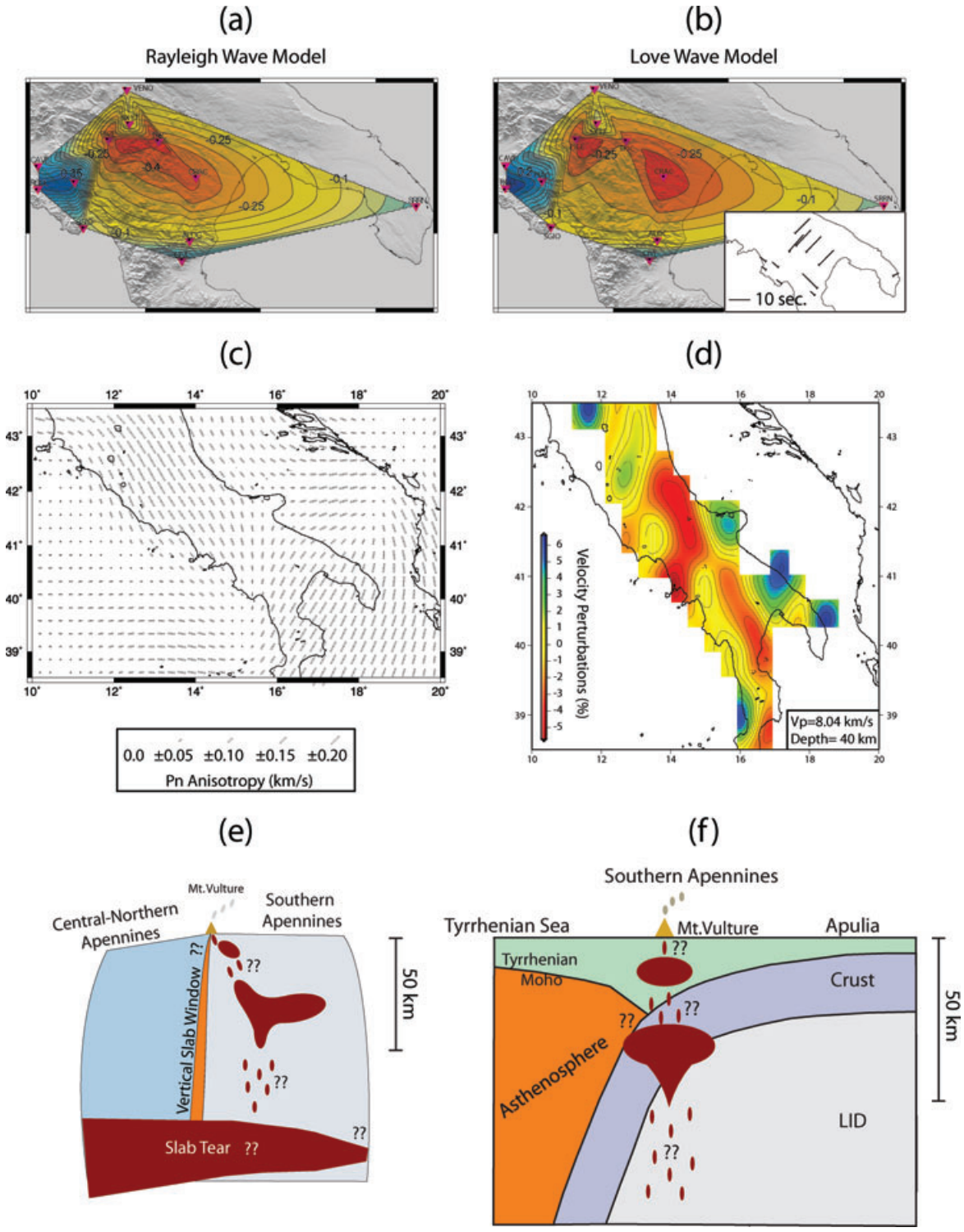

Figure 17. Perturbation of wave speeds at 40 km depth for (a) vertically polarized and (b) SH-polarized waves. The map inset shows the fast azimuthal anisotropy direction obtained from radial- and transverse-component surface waves. (c) Fast propagation directions are consistent between Pn (Mele *et al.* 1998) and the horizontal-component surface waves. (d) *P* velocity variation (at 40-km depth; Cimini & De Gori 2001) provides further evidence of low velocities beneath the Apennines. (e) Interpretative cross-section along the southern Apennine based on this analysis. (f) Interpretative cross-section perpendicular to the Apennines. The low-velocity zones are caused by hot (potentially wet) asthenospheric material beneath the study region.

mafic (therefore faster), a scenario that can be effectively ruled out considering the prevailing evidence of the low-velocity zones at the hypothesized lower-crustal depths. The modest mantle velocities (4.1–4.3 km s^{-1}) at ∼50-km depths suggest an upper mantle origin. That is, asthenospheric upwelling of hot, possibly molten, material could interact with the base of the crust and produce a weak crust–mantle interface and a low-velocity body within the crust.

In short, partial melting could be an important process beneath the southern Apennines. Without the involvement of partial melt, a shear velocity perturbation of –0.35 km s^{-1} would require an

unrealistic thermal variation of ∼900 °C (Forsyth 1992; Nataf & Ricard 1996). Furthermore, a solid asthenosphere is simply incompatible with the anomalous attenuation of Sn and Pn waves beneath the Apennines (Mele *et al.* 1996, 1997, 1998). On the other hand, the presence of 5–6 per cent of partial melt distributed in tubes, 3–4 per cent of partial melt in penny-shaped sections, or less than 1 per cent of partial melt in thin films with an aspect ratio of 0.01 (Forsyth 1992; Faul *et al.* 1994; Hung *et al.* 2000), could all reduce shear velocities by ∼0.5 km s^{-1} (observed) or more. More recently, Hammond & Humphreys (2000) stipulated that 1 per cent of melt in cuspate and naturally organized melt inclusion could give rise to a 7.9 per cent decrease in shear velocities. Based on this assumption, less than 2 per cent partial melt is needed to explain the observed 0.5 km s^{-1} velocity perturbation beneath the southern Apennines. Slab tear and/or break-off near crustal depths, as suggested by the recent work of Yoshioka & Wortel (1995), Wong a Ton & Wortel (1997) and Van der Zedde & Wortel (2001), offer attractive mechanisms for the extrusion of partial melt to relatively shallow depths. Unfortunately, the poor vertical resolution of surface waves at depth below 50 km greatly hampers our ability to decipher the connection between partial melting at crustal depths and the deeper source(s) of mantle upwelling.

Further support of a partially molten crustal layer comes from recent geological and geochemical data. As shown by Fig. 10, the low-velocity zone shallows towards the northwestern corner of the study area, which is less than 30 km southeast of Mt Vulture—a once-active volcano located close to the outskirt of Apennine thrust belt. Generally classified as a member of the Intramontane Ultra-alkaline Province (Lavecchia & Stoppa 1996; Lavecchia *et al.* 2006), Mt Vulture is rich in Ca-carbonatites and potassic mellilite (kamafugite)—two minerals that are frequently found in continental rift zones such as the East-African Rift System, or intra-plate extensional regimes similar to Western Qinling, Gansu Province, China (Bailey 1993; Bell *et al.* 1999; Bailey & Collier 2000; Woolley 2003; Yu *et al.* 2003; Lavecchia *et al.* 2006). D'Orazio *et al.* (2007) used a vertical slab window hypothesis to explain that Mt Vulture might be alimented by mantle material (Fig. 17e). While this hypothesis implies vertical transport of partially molten asthenospheric material, it is plausible that an initially vertical intrusion could end up broadening and propagating along the Apenninic chain within the lower-pressure, extensional regimes at crustal depths. Without further data constraints, both extension-based and gap-based mechanisms for asthenospheric flow offer possible explanations for the anomalously slow crustal shear velocities at 6–12 km depth.

5 CONCLUSIONS

Modelling of surface wave waveforms in wide time windows requires undivided attention not only to fundamental modes, but to the reverberative energy that results from higher overtones and/or coupling between mode branches. In this study, we simultaneously analysed three-component surface waves using two of the largest ($M_w > 5$) regional earthquakes that took place near Italy during the CAT/SCAN experiment. The main conclusions of our study are best illustrated by simple schematic diagrams of mantle processes along and across southern Apennines (Figs 17e and f) based on the surface wave modelling. Our main observations are summarized as follows.

1. Waveforms provide convincing evidence for a major tectonic boundary separating Apulia, a high-velocity region, and the southern Apennines.

2. A prominent low-velocity layer exists beneath the southern Apennines orogenic front at depths below 30 km. This layer is at least 15 km thick and could potentially extend to larger depths.

3. The aforementioned low-velocity layer is strongly anisotropic. The fast surface wave propagation direction approximately aligns with the NE–SW extension axis east of the mountain front.

4. We interpret the NW–SE trending low-velocity, anisotropic zone as potential evidence of partial melting due to asthenospheric upwelling in this region. The presence of this anomaly may be associated with a deeper melting zone through processes such as slab detachment or tear. The potential existence of slab windows and the low-pressure extensional crustal environment could also be important.

ACKNOWLEDGMENTS

We thank Alessandro Amato, Andrea Morelli, and Claudio Chiarabba for insightful scientific discussions. We are grateful that Giovanni Battista Cimini and Giuliana Mele kindly sent their published models for comparisons. Keith Brzak and Stephen Bannister assisted us during the preparation of this manuscript. Comments and suggestions provided by Lapo Boschi and an anonymous reviewer helped to improve the quality of the paper. The data were made available by IRIS Data Management Centre. This research is funded by NSERC, Alberta Ingenuity and the Canadian Foundation for Innovations. This work was partially funded by National Science Foundation grant EAR 99-10554 and EAR 06-07687, Lamont-Doherty Earth Observatory publication 7262.

REFERENCES

Amato, A., Alessandrini, B. & Cimini, G.B., 1993. Teleseismic tomography of Italy, in *Seismic Tomography: Theory and Applications,* pp. 361–396, eds Iyer H.M., Hirahara, K., Prentice-Hall, London.

Baccheschi, P., Margheriti, L. & Steckler, M.S., 2007. Seismic anisotropy reveals focused mantle flow around the Calabrian slab (Southern Italy), *Geophys. Res. Lett.,* **34,** L05302, doi:10.1029/2006/GL028899.

Bailey, D.K., 1993. Carbonate magmas, *J. Geol. Soc. Lond.,* **150,** 637–651.

Bailey, D.K. & Collier, J.D., 2000. Carbonatite-melilite association in the Italian collision zone and Ugandan rifted craton: significant common factors, *Mineral. Mag.,* **64,** 675–682.

Barberi, G., Cosentino, M.T., Gervasi, A., Guerra, I., Neri, G. & Orecchio, B., 2004. Crustal seismic tomography in the Calabrian Arc region, south Italy, *Phys. Earth planet. Inter,* **147,** 297–314.

Bell, K., Kjarsgaard, B.A. & Simonetti, A., 1999. Carbonatites into the twenty-first century, *J. Petrol.,* **39,** 1839–1845.

Bijwaard, H., Spakman, W. & Engdahl, R., 1998. Closing the gap between regional and global travel time tomography, *J. geophys. Res.,* **103,** 30 055–30 078.

Boschi, L., Ekström, G. & Kustowski, B., 2004. Multiple resolution surface wave tomography: the Mediterranean basin, *Geophys. J. Int.,* **157,** 293–304.

Boschi, L., Fry, B., Ekström, G. & Giardini, D., 2008. The European upper mantle as seen by surface waves, *Surv. Geophys.,* in revision.

Carminati, E., Wortel, M.J.R., Spakman, W. & Sabadini, R., 1998. The role of slab detachment processes in the opening of the western-central Mediterranean basins: some geological and geophysical evidence, *EPSL,* **160,** 651–665.

Cavaza, W., Roure, F. & Ziegler, P.A., 2004. The Mediterranean area and the sourrounding regions: active processes, remnants of former Tethyan oceans and related thrustbelts, in *The TRANSMED Atlas—The Mediterranean Region from Crust to Mantle,* eds Cavazza, V., Roure, F., Spakman, W., Stampfli, W., Ziegler, P.A., Springer, Berlin Heidelberg.

Červený, V., Klimeš, L. & Pšenčík, I., 1984. Paraxial ray approximations in the computation of seismic wavefields in inhomogeneous media, *Geophys. J. Roy. astron. Soc.,* **79,** 89–104.

Cimini, G. & De Gori, P., 2001. Nonlinear P-wave tomography of subducted lithosphere beneath central-southern Apennines (Italy), *Geophys. Res. Lett.,* **22,** 4387–4390.

Civello, S. & Margheriti, L., 2004. Toroidal mantle flow around the Calabrian slab (Italy) from SKS splitting, *Geophys. Res. Lett.,* **31,** L10601, doi: 10.1029/2004GL019607.

Chiarabba, C. & Amato, A., 1996. Crustal velocity structure of the Apennines (Italy) from P-wave travel time tomography, *Ann. Geophys.,* **39,** 1133–1148.

Chiarabba, C., Jovane, L. & DiStefano, R., 2005. A new view of Italian seismicity using 20 years of instrumental recordings, *Tectonophysics,* **295,** 251–268.

D'Agostino, N. & McKenzie, D., 1999. Convective support of long-wavelength topography in the Apennines (Italy), *Terra Nova,* **11,** 234–238.

D'Orazio, M., Innocenti, F., Toarini, S. & Doglioni, C., 2007. Carbonatites in a subduction system: the Pleistocene alvikites from Mt. Vulture (southern Italy), *Lithos,* **98,** 313–334.

de Jonge, M.R., Wortel, M.J.R. & Spakman, W., 1994. Regional scale tectonic evolution and the seismic velocity structure of the lithosphere and upper mantle: the Mediterranean region, *J. geophys. Res.,* **99,** 12 091–12 108.

Dézes, P., Ziegler, P.A., 2002. Moho depth map of Western and Central Europe, World Wide Web Address: http://www.unibas.ch/eucor-urgent.

Di Stefano, R., Chiarabba, C., Lucente, F. & Amato, A., 1999. Crustal and upper-most mantle structure in Italy from inversion of P-wave arrival times: geodynamic implications, *Geophys. J. Int.,* **139,** 483–498.

Dziewonski, A.M. & Anderson, D.L., 1981. Preliminary reference Earth model, *Phys. Earth planet. Inter.,* **25,** 297–356.

Dziewonski, A.M., Chou, T.-A. & Woodhouse, J.H., 1981. Determination of earthquake source parameters from waveform data for studies of global and regional seismicity, *J. geophys. Res.,* **86,** 2825–2852.

Faul, U.H., Toomey, D.R. & Waff, H.S., 1994. Intergranular basaltic melt is distributed in thin, elongated inclusions, *Geophys. Res. Lett.,* **21**(1), 29–32.

Forsyth, D.W., 1992. Geophysical constraints on mantle flow and melt migration beneath mid-ocean ridges, in *Mantle Flow and Melt Generation at Mid-ocean Ridges*, *Geophys. Monogr. Ser.,* Vol. **71**, pp. 1–65, eds Phipps Morgan, J. Blackman, D.K. Sinton, J.M. AGU, Washington, DC.

Fuchs, K. & Müller, G., 1971. Computation of synthetic seismograms with the reflectivity method and comparisons with observations, *Geophys. J. R. astr. Soc.,* **23,** 417–433.

Gu, Y.J., Webb, S.C., Lerner-Lam, A. & Gaherty, J.B., 2005. Upper mantle structure beneath the eastern Pacific Ocean ridges, *J. geophys. Res.,* **110,** B06305, doi:10.1029/2004JB003381.

Gu, Y.J., 2006. Probing the history of the Mathematician Paleoplate using surface waves, *Tectonophysics,* **424,** 41–51.

Gudmundson, O. & Sambridge, M., 1998. A regionalized upper mantle (RUM) seismic model, *J. geophys. Res.,* **103,** 7121–7136.

Hammond, W.C. & Humphreys, E.D., 2000. Upper mantle seismic wave velocity: effects of realistic partial melt geometries, *J. geophys. Res.,* **105**(B5), 10 975–10 986.

Herrmann, R.B. & Wang, C.Y., 1985. A comparison of synthetic seismograms, *Bull. seism. Soc. Am.,* **75,** 41–56.

Hippolyte, J.C, Angelier, J. & Roure, F., 1994. A major geodynamic change revealed by quaternary stress patterns in the southern Apennines (Italy), *Tectonophysics,* **230,** 199–210.

Hollenstein, C., Kahle, H.G., Geiger, A., Jenny, S. & Giardini, D., 2003. New GPS constraints on the Africa-Eurasia plate boundary zone in southern Italy, *Geophys. Res. Lett.,* **30**(18), 1935, doi:10.1029/2003GL017554.

Hung, S.H., Forsyth, D.W. & Toomey, D.R., 2000. Can a narrow, melt-rich, low-velocity zone of mantle upwelling be hidden beneath the East Pacific Rise? Limits from waveform modeling and the MELT Experiment, *J. geophys. Res.,* **105**(B4), 7945–7960.

Kennett, B.L.N., 1975. The effects of attenuation on seismograms, *Bull. seism. Soc. Am.,* **65,** 1643–1651.

Kennett, B.L.N., 1979. Theoretical reflection seismograms for an elastic medium, *Geophys. Prospect.,* **27,** 301–321.

Kennett, B.L.N.,1983. *Seismic Wave Propagation in Stratified Media,* pp. 342, Cambridge University Press, Cambridge, New York.

Kennett, B.L.N., 1991. *IASPEI 1991 Seismological Tables,* pp. 167, Research School of Earth Sciences, Canberra, Australia.

Kind, R., 1976. Computation of reflection coefficients for layered medium, *Geophysics,* **41,** 191–200.

Kind, R., 1978. The reflectivity method for a buried source, *J. Geophys.,* **44,** 603–612.

Lavecchia, G. & Stoppa, F., 1996. The tectonic significance of Italian magmatism: an alternative view to the popular interpretation, *Terra Nova,* **8,** 435–446.

Lavecchia, G., Stoppa, F. & Creati, N., 2006. Carbonatites and kamafugites in Italy: mantle-derived rocks that challenge subduction, *Ann. Geophys.,* **49,** 389–402.

Levin, V., Park, J., Lucente, F.P., Margheriti, L. & Pondrelli, S., 2007. End of subduction in northern Apennines confirmed by observations of quasi-Love waves from the great 2004 Sumatra-Andaman earthquake, *Geophys. Res. Lett.,* **34,** L04304, doi:10.1029/2006GL028860.

Lucente, F.P., Chiarabba, C., Cimini, G.B. & Giardini, D., 1999. Tomographic constraints on the geodynamic evolution of the Italian region, *J. geophys. Res,* **104**(B9), 20 307–20 327.

Margheriti, L., Lucente, F.P. & Pondrelli, S., 2003. SKS splitting measurements in the Apenninic-Tyrrhenian domain (Italy) and their relation with lithospheric subduction and mantle convection, *J. geophys. Res.,* **108**(B4), 2218, doi:10.1029/2002JB001793.

Marone, F., Van Der Meijde, M., Van Der Lee, S. & Giardini, D., 2003. Joint inversion of local, regional and teleseismic data for crustal thickness in the Eurasia-Africa plate boundary region, *Geophys. J. Int.,* **154,** 499–514.

Marquering, H. & Snieder, R., 1996. Shear-wave velocity structure beneath Europe, the northeastern Atlantic and Asia from waveform inversions including surface-wave mode coupling, *Geophys. J. Int.,* **127,** 283–304.

Meissner, R., Wever, T. & Flüh, E., 1987. The Moho in Europe—implications for crustal development, *Ann. Geophys.,* **5B,** 357–364.

Mele, G., Rovelli, A., Seber, D. & Barazangi, M., 1996. Lateral variations of Pn propagation in Italy: evidence for a high-attenuation zone beneath the Apennines, *Geophys. Res. Lett.,* **23**(7), 709–712.

Mele, G., Rovelli, A., Seber, D. & Barazangi, M., 1997. Shear wave attenuation in the lithosphere beneath Italy and surrounding regions: tectonic implications, *J. geophys. Res.,* **102**(B6), 11 863–11 875.

Mele, G., Rovelli, A., Seber, D., Hearn, T.M. & Barazangi, M., 1998. Compressional velocity structure and anisotropy in the uppermost mantle beneath Italy and surrounding regions, *J. geophys. Res.,* **103,** 12 529–12 543.

Meletti, C., Patacca, E. & Scandone, P., 2000. Construction of a seismotectonic model: the case of Italy, *Pure appl. Geophys.,* **157,** 11–35.

Menardi Noguera, A. & Rea, G., 2000. Deep structure of the Campanian-Lucanian Arc (Southern Apennine, Italy), *Tectonophysics,* **324,** 239–265.

Metropolis, N. & Ulam, S., 1949. The Monte Carlo method, *J. Am. Stats. Assoc.,* **44,** 247, 335–341, doi:10.2307/2280232.

Montone, P., Mariucci, M.T., Pondrelli, S. & Amato, A., 2004. An improved stress map for Italy and surrounding regions (central Mediterranean), *J. Geophys. Res.-Solid Earth,* **109,** B10410. doi:10.1029/2003JB002703.

Montuori, C., Cimini, G.B. & Favali, P., 2007. Teleseismic tomography of the southern Tyrrhenian subduction zonenew results from seafloor and land recordings, *J. geophys. Res.,* **112,** B03311, doi:10.1029/2005JB004114.

Nataf, H.C. & Ricard, Y., 1996. 3SMAC: an a priori tomographic model of the upper mantle based on geophysical modeling, *Phys. Earth planet. Inter.,* **95,** 101–122.

Panza G.F., Pontevivo, A., Chimera, G., Raykova, R. & Aoudia, A., 2003. The lithosphere-asthenosphere: Italy and surroundings. *Episodes,* **26**(3), 169–172.

Panza, G.F., Peccerillo, A., Aoudia, A. & Farina, B., 2007. Geophysical and petrological modelling of the structure and composition of the crust and

upper mantle in complex geodynamic settings: the Tyrrhenian Sea and surroundings, *Earth-Sci. Rev.,* **80,** 1–46.

Pasyanos, M.E. & Walter, W.R., 2002. Crust and upper-mantle structure of North America, Europe and the Middle East from inversion of surface waves, *Geophys. J. Int.,* **149,** 463–481.

Pentevivo, A. & Panza, G.F., 2002. Group velocity tomography and regionalization in Italy and bordering areas, *Phys. Earth planet. Inter.,* **134,** 1–15.

Pentevivo, A. & Panza, G.F., 2006. Lithosphere-asthenosphere system in the Calabrian Arc, *Pure applied Geophys.,* **163,** 1617–1659.

Piromallo, C. & Morelli, A., 1997. Imaging the Mediterranean upper mantle by P-wave travel time tomography, *Ann. Geophys.,* **40,** 963–979.

Piromallo, C. & Morelli, A., 2003. P wave tomography of the mantle under the Alpine-Mediterranean area, *J. geophys. Res.,* **108**(B2), 2065, doi:10.1029/2002JB001757.

Pondrelli, S., Morelli, A., Ekström, G., Mazza, G., Boschi, E. & Dziewonski, A.M., 2002. European-Mediterranean regional centroid-moment tensors: 1997–2000, *Phys. Earth planet. Inter,* **130,** 71–101.

Pondrelli, S., Salimbeni, S., Ekström, G., Morelli, A., Gasperini, P. & Vannucci, G., 2006. The Italian CMT dataset from 1977 to the present, *Phys. Earth planet. Inter,* **159,** 286–303.

Randall, G.E., 1994. Efficient calculation of complete differential seismograms for laterally homogeneous Earth models, *Geophys. J. Int.,* **118,** 245–254.

Raykova, R. & Nikolova, S., 2007. Tomography and velocity structure of the crust and uppermost mantle in southeastern Europe obtained from surface wave analysis, *Stud. Geophys. Geod.,* **51**(1), 165–184.

Rosenbaum, G. & Lister, G.S., 2004. Formation of arcuate orogenic belts in the western Mediterranean region, in *Orogenic Curvature: Integrating Paleomagnetic and struCtural Analyses,* Vol. 383, pp. 41–56, eds Sussman, A.J. And Weil, A.B., *Geological Society of America Special Paper,* Boulder, Colarado.

Scrocca, D., Carminati, E. & Doglioni, C., 2005. Deep structure of the southern Apennines, Italy: thin-skinned or thick-skinned?, *Tectonics,* **24,** TC3005, doi:10.1029/2004TC001634.

Selvaggi, G. & Chiarabba, C., 1995. Seismicity and P-wave velocity image of the Southern Tyrrhenian subduction zone, *Geophys. J. Int.,* **121,** 818–826.

Serpelloni, E., Anzidei, M., Baldi, P., Casula, G. & Galvani, A., 2005. Crustal velocity and strain-rate fields in Italy and surrounding regions: new results from the analysis of permanent and non-permanent GPS networks, *Geophys. J. Int.,* **161,** 861–880.

Serpelloni, E., Anzidei, M., Baldi, P., Casula, G. & Galvani, A., 2006. GPS measurement of active strains across the Apennines (Italy), *Ann. Geophys.,* **49,** 319–329.

Silver, P.G., 1996. Seismic anisotropy beneath the continents: probing the depths of geology, *Annu. Rev. Earth planet Sci.,* **24,** 385–432.

Snieder, R., 1988. Large scale waveform inversions of surface waves for lateral heterogeneity, 2: application to surface waves in Europe and Mediterranean, *J. geophys. Res.,* **93,** 12 067–12 080.

Solaro, G., Tizzani, P., Milano, G. & Pauselli, C., 2007. Rheological behavior of the crust in the Southern Apennines (Italy): results from a thermal and seismological study, *Terra Nova,* **19,** 353–359, doi:10.1111/j.1365–3121.2007.00759.x.

Spakman, W., Van Der Lee, S. & Van Der Hilst, R., 1993. Travel-time tomography of the European-Mediterranean mantle down to 1400 km, *Phys. Earth planet. Inter.,* **79,** 3–74.

Spakman, W. & Wortel, M.J.R., 2004. A tomographic view on Western Mediterranean geodynamics, in *The TRANSMED Atlas – The Mediterranean Region from Crust to Mantle,* pp. 31–52, eds Cavazza, V., Roure, F., Spakman, W., Stampfli, W., Ziegler, P.A., Springer, Berlin Heidelberg.

Stampfli, G.M. & Borel, G.D., 2004.The TRANSMED transects in space and time: constraints on the paleotectonic evolution of the Mediterranean domain, in *The TRANSMED Atlas – The Mediterranean Region from Crust to Mantle,* pp. 53–80, eds Cavazza, V., Roure, F., Spakman, W., Stampfli, W. Ziegler, P.A., Springer, Berlin Heidelberg.

Steckler, M.S., Agostinetti, N.P., Wilson, C.K., Roselli, P., Seeber, L., Amato, A. & Lerner-Lam, A., 2008. Crustal structure in the southern Apennines from teleseismic receiver functions, *Geology,* **36,** 155–158.

Stich, D. & Morelli, A., 2007. Reflection of seismic surface waves at the northern Apennines, *Earth planet. Sci. Lett.,* **259,** 149–158.

Tiberti, M.M., Orlando, L., Di Bucci, D., Bernabini, M. & Parotto, M., 2005. Gravity anomaly map and crustal model of the Central-Southern Apennines (Italy), *J. Geodyn.,* **40,** 73–91.

Van Der Zedde, D.M.A. & Wortel, M.J.R., 2001. Shallow slab detachment as a transient source of heat at mid-lithospheric depths, *Tectonics,* **20,** 868–882.

Venisti, N., Calcagnile, G., Pontevivo, A. & Panza, G.F., 2005. Tomographic study of the Adriatic Plate, *Pure appl. Geophys.,* **162,** 311–329.

Voigt, V., 1928. *Lehrbuck der Kristallphysik,* Teubner, Leipzig, 929 pp.

Wong A., Ton, S.Y.M. & Wortel, M.J.R., 1997. Slab detachment in continental collision zones: an analysis of controlling parameters, *Geophys. Res. Lett.,* **24**(16), 2095–2098.

Woolley, A.R., 2003. Igneous silicate rocks associated with carbonatites: their diversity, relative abundances and implications for carbonatite genesi, *Period. Miner.,* **1,** 9–17.

Wortel, M.J.R. & Spakman, W., 1992. Structure and dynamics of subducted lithosphere in the Mediterranean region, *Proc. K. Ned. Akad. Wet.,* **95,** 325–347.

Wortel, M.J.R. & Spakman, W., 2000. Subduction and slab detachment in the Mediterranean-Carpathian region, *Science,* **290,** 1910–1917.

Yomogida, K., 1992. Fresnel zone inversion for lateral heterogeneities in the Earth, *Pure appl. Geophys.,* **138,** 391–406.

Yoshioka, S. & Wortel, M.J.R., 1995. Three-dimensional numerical modeling of detachment of subducted lithosphere, *J. geophys. Res.,* **100,** 20 223–20 244.

Yu, X., Mo, X., Liao, Z, Zhao, X. & Su, Q., 2003. Geochemistry of kamafugites and carbonatites from West Qinling area (China), *Period. Miner.,* **1,** 161–179.

Zhou, Y., Nolet, G., Dahlen, F.A. & Laske, G., 2006. Global upper-mantle structure from finite-frequency surface-wave tomography, *J. geophys. Res.,* **111,** B04304, doi:10.1029/2005JB003677.